DETECTION OF HARD BETA RAYS IN WATER THROUGH THE CERENKOV EFFECT

B. Turck

Translation of "Detection des β Durs dans L'Eau par Effet Cerenkov."

Commissariat a l'Energie Atomique, Centre d'Etudes Nucleaires, Saclay (France), Report CEA R-2915, 1966, 66 pp

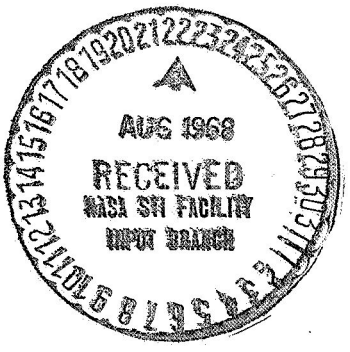

NATIONAL AERONAUTICS AND SPACE ADMINISTRATION
WASHINGTON, D. C. 20546 AUGUST 1968

THESES

Presented

TO THE SCIENCE DEPARTMENT OF THE

UNIVERSITY OF PARIS

D'Orsay Center

In fulfilment of the requirements for the title of Doctor-Engineer

of the Physical Sciences

by

BERNARD TURCK

FIRST THESIS: Detection of Hard Beta Rays in Water Through the Cerenkov Effect

SECOND THESIS: Recommendations of the Department

Defended 28 January, 1965 before the Examination Commission

MM. RIOU, President,

MM. UEBERSFELD AND BLANC, Examiners

To Monsieur Jean Teillac, who has been my guide in this work, I respectfully express my gratitude.

I would like also to thank Messieurs Jacques Labeyrie and André Blanc of the Saclay Center of Nuclear Studies for their valuable advice.

To Monsieur Alain Lansiart, who has followed the development of this work with close attention, I would like to express my thanks.

TABLE OF CONTENTS

DETECTION OF HARD BETA RAYS IN WATER THROUGH THE CERENKOV EFFECT

B. Turck

ABSTRACT: Describes equipment capable of detecting $8 \cdot 10^{-8}$ μc/cc of strontium – yttrium 90 in water (i.e., one-tenth of the maximum permissible concentration) within a time of few minutes. This equipment is especially useful for monitoring water quality, because it is simple to manufacture and operate. Moreover, the apparatus permits identification of some individual radioactive elements in water by means of an energy. discrimination technique.

INTRODUCTION

/7*

The increase in rainwater and rivers of pollutive fission products from reactor discharge and nuclear explosion fallout, has impelled us to design detectors that are simple to use. Such a device need not require special treatment of drinking water such as evaporation or the concentration of mineral salts. We have considered measuring directly the activity of radioactive beta-ray emitters in clear water, at the level of the least detectable concentration by using the Cerenkov light emitted on the passage of the particle.

A patent based on this method has already been taken out by the Society of the Industrial Applications of Physics [27]. The method has also been the subject of several applied papers [1, 2]. It is direct, a priori very sensitive, and lends itself to continuous monitoring.

Strontium 90 is one of the most dangerous to life of the fission products. The detectors described in the literature cited, however, the sensitivity was so low that it did not provide, in particular, precise information on strontium 90 contamination at the tolerance dose level ($8 \cdot 10^{-7}$ μc/cc, (Official Journal, 11 July 1957).

One of these methods [1] utilized two fast–response photomultipliers in a coincidence circuit to reduce the effect of photocathode thermionic noise. The volumes tested were very low, however (20 cm^3). In attempts made by the Japanese [2], the concidence photomultipliers did not have a sufficiently fast response, the noise level was too high, and the photocathodes had to be cooled. The volume tested, however, was much larger.

Taking these studies into account, together with the fact that experiment has demonstrated the possibility of collecting emitted light with coarse scintillators without too much photon loss, we have investigated equipment using fast–response photomultipliers in coincidence, and observed the light given off by a large volume of weakly active water (on the order of a liter). The various factors involved in sensitivity limitation

*Numbers in the margin indicate pagination in the foreign text.

were studied, and we succeeded in developing equipment much improved in sensitivity, in convenience of operation, and in the quantitative and selective measurement of the contamination.

/8

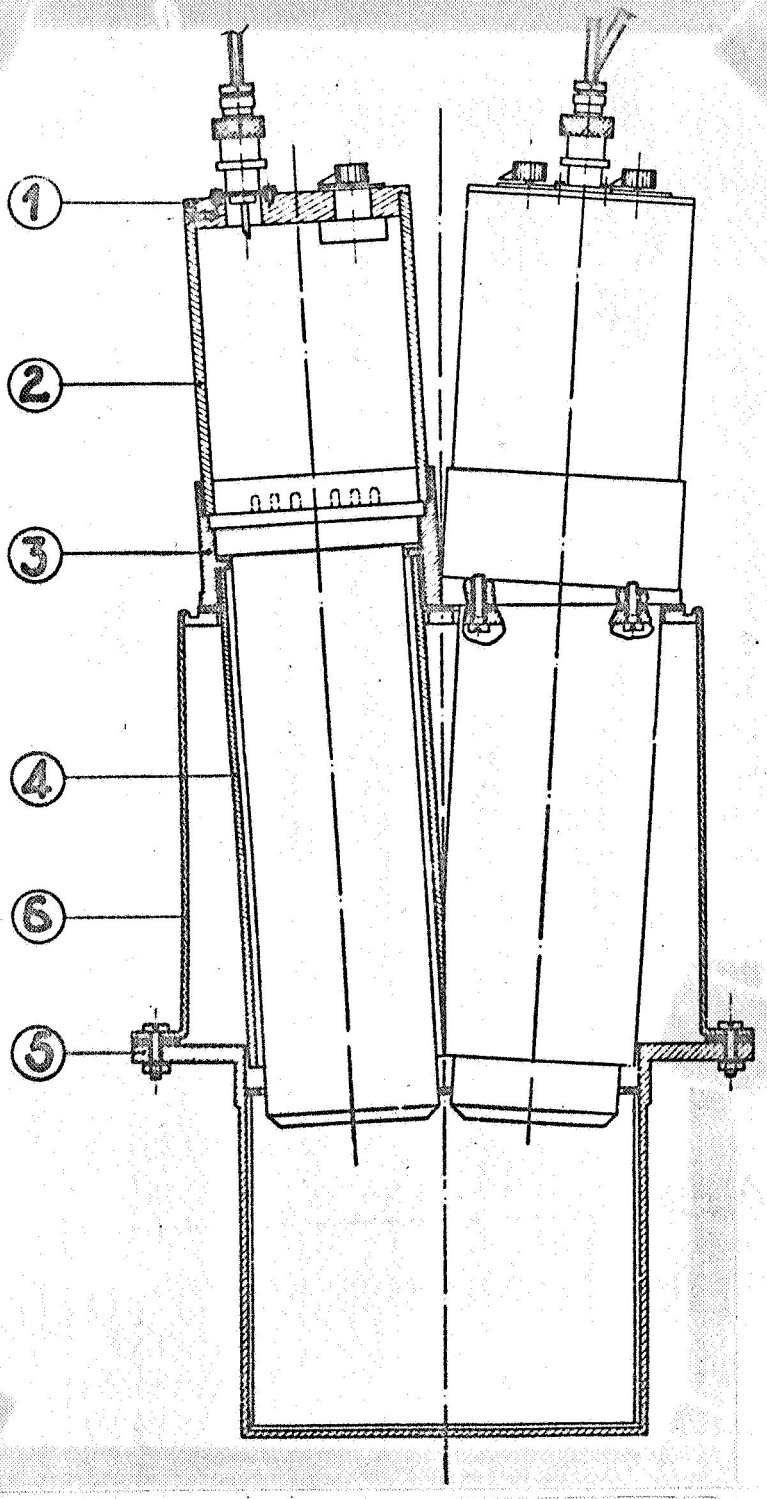

Legend: 1) Lid; 2) Upper cylinder; 3) Cylinder casing; 4) Lower cylinder; 5) Tank; 6) Support for photomultiplier assembly.

Figure 1. Equipment for Detection by means of the Cerenkov effect.

I. THEORETICAL YIELD /9*

1. Light Emitted by the Passage of a Particle Through Water.

The phenomenon of light emission in irradiated transparent media was established in 1928 by Malet. It was not until 1937, however, that Cerenkov and later Frank and Tamm explained it by the electromagnetic theory of light [3, 4].

From the macroscopic point of view, it may be said that the medium is locally polarized upon passage of the particle. In returning to their original state, the molecules emit photons retaining the same polarization; these combine or are annihilated, depending on the velocity of the particle.

If we consider a charged particle moving in the x direction at a velocity v inside a homogeneous and isotropic medium; the resultant perturbation is propagated as a sphere with its center at 0 and a velocity of c/n, where c is the velocity of light in vacuum ($3 \cdot 10^{10}$ cm/sec), and n is the medium's index of refraction (1.34 for water).

If the time taken by the particle in moving from 0 to M is equal to that taken by the light perturbation in moving from 0 to H, all the waves will then arrive in phase along the straight line HM. This line is the generatrix of a cone of revolution which constitutes an envelope moving in the 0H direction with a velocity c/n. The direction of propagation is then given by $\cos \theta = 1/\beta n$, where $\beta = v/c$ (Fig. 2).

The condition for the existence of the radiation is $\beta n > 1$; i.e., that there exists a velocity with a lower limit of β equal to 1/n (0.75 for water). The velocity is related directly to the kinetic energy by

$$E = m_0 c^2 [(1 - \beta^2)^{-1/2} - 1]$$

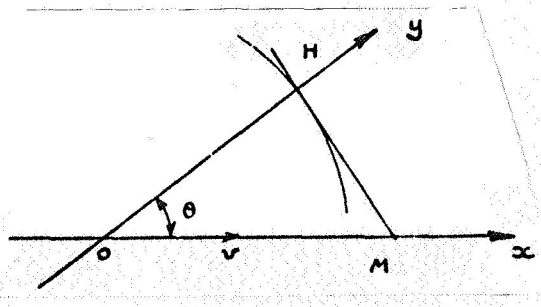

Figure 2. Cerenkov Emission in a Transparent Medium.

from which the Cerenkov threshold in water may be derived for various particles.

With the deceleration of the electrons, resulting from energy losses via bremsstrahlung and especially via ionization, the trajectory does not remain rectilinear. The radiation changes direction, but the sum total of the light is not affected provided it is emitted at every point in the medium. /10*

Frank and Tamm [5] calculated the energy dW radiated by an electron moving at constant velocity on a path dl in a perfect dielectric:

Particle	Electron	Meson μ	Pi Meson π	K meson	Proton
E MeV thresh	0.26	50	68	220	46C

$$\frac{dW}{dl} = \frac{e^2}{c^2}\int_{\beta n>1}\left(1 - \frac{1}{\beta^2 n^2}\right)\omega\, d\omega$$

where e is the charge of the electron, and ω is the frequency of the emitted light. This expression diverges as the frequency spectrum extends from zero to infinity. In fact, the medium is refractive, and the index of the water is a function of ω in accordance with:

$$n^2 = 1 - \frac{A}{\omega_0^2 - \omega^2}$$

in a narrow band, where the integral becomes directional.

More elaborate expressions like that of Ginsburg [6], which is obtained by a quantum-mechanical treatment of the problem, lead to formulas differing only slightly from the preceding expression over o–frequency range limited to visible light and the near–ultra-violet.

The radiated energy is expressed by

$$\frac{dW}{dl} = 4\pi^2 e^2 \int_{\beta n>1}\left(1 - \frac{1}{\beta^2 n^2}\right)\frac{d\lambda}{\lambda^3}$$

from which we can derive an expression for the number of photons emitted per centi-meter of the path:

$$\frac{dN}{dl} = \frac{4\pi^2 e^2}{hc}\int_{\beta n>1}\left(1 - \frac{1}{\beta^2 n^2}\right)\frac{d\lambda}{\lambda^2} = 2\pi\alpha \int\left(1 - \frac{1}{\beta^2 n^2}\right)\frac{d\lambda}{\lambda^2} = 2\pi\alpha\int C(\lambda)d\lambda$$

where α is fine structure constant $2\mu e^2/hc$, which is 1/137 in cgs units, and $C(\lambda)$ is the Cerenkov spectrum

$$C(\lambda) = \left[1 - \frac{1}{\beta^2 n^2(\lambda)}\right]\frac{1}{\lambda^2}$$

The number of photons emitted in the band $d\lambda$ varies as $1/\lambda^2$. It would seem interesting, then, to direct our attention to the short wavelengths.

2. Detector Characteristics

Since the water to be studied is the very medium in which the Cerenkov effect is produced, the entire volume must have the same properties, and the radiation near a photocathode, for example, cannot be emitted at a higher yield than that emitted at some distance from it. The fact that the two photomultipliers are coincident reduces this inequality substantially.

Thus, if p_1 and p_2 are the probabilities of detection for each photomultiplier, the detection probability of the two in coincidence is $p_1 p_2$. For an electron emitted at the bottom of the apparatus, p_1 and p_2 are equal; however, if an electron is emitted in the neighborhood of a photocathode, and the yield p_1 of the corresponding photomultiplier

becomes very large; p_2, by contrast, becomes very small, and thus the product $p_1 p_2$ varies only slightly. We have verified this experimentally.

The vessel containing the emitting medium is a cylindrical one-liter tank. Its almost equal dimensions (115 mm in diameter, 100 mm deep) should ensure a good yield. Indeed, this yield is a maximum in cylindrical scintillators in which the depth and diameter are equal.

The two photomultipliers are arranged vertically and reach the surface of the water through two holes, the remainder of the internal surface of the vessel being reflective (metal) or diffusive (paint).

To determine the detection probability $p_d = p_1 p_2$ for a beta ray, we shall assume /11
that p_1 and p_2 are equal, on the average. They depend on:

a) the number of photons emitted, i.e., the beta energy;
b) the light collection factor:
c) the quantum yield of the photocathodes and of the counting threshold.

We begin by determining the optical yield of the tank; i.e., the ratio between the number of photons incident on one of the photocathodes to the number of photons emitted by the Cerenkov effect.

3. Evaluation of the Optical Yield of the Detector

To simplify the computations, we assume the vessel containing the medium to be a sphere of the same volume. If a is the radius of the cylinder, the radius of the sphere will be $r = 1.2\,a$ (Fig. 3).

The light emitted in the medium reaches a photocathode either directly or after a certain number of reflections from the walls. At any given wave-length, we define the following quantities:

a) the absorption per centimeter of the water (Fig. 5). The number of photons surviving a passage of path x is [7]

$$N(x) = N(0)\exp(-\mu x)$$

b) the reflection coefficient (specular or diffuse) of the walls. In the case of a metallic surface, the reflection coefficient depends on the angle of incidence and on the metal. We shall later show that a perfectly diffusing surface permits collection of all the light. This is not the case for perfect mirrors, where a ray emitted by a point on the sphere always remains trapped within the same great circle. In our calculations, we choose a priori a coefficient of reflection $R(\lambda)$ which corresponds closely to the best materials that might conceivably be used [3], (Fig. 4).

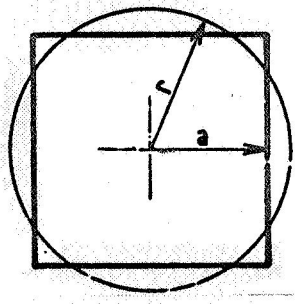

Figure 3. Sphere Equivalent to the Detector.

Let ΔS be the collecting surface and S be the total surface of the sphere. If n is the number of photons impinging on the photocathodes, and N the number of photons emitted in the medium, the optical yield is $\eta = n/2N$ for each photomultiplier.

a. Flux Leaving the Diffusing Sphere.

Since the surface ΔS is a twentieth of the total surface S, we can compare the spherical segment ΔS to the circular cross section. We shall also suppose that the radiation obeys Lambert's law.

The emitted light is uniformly distributed over the sphere. The flux leaving directly from ΔS is independent of the location of this element, so that /13

$$Nt\,\frac{\Delta S}{S}$$

is collected. Here, t is the mean transmission coefficient between an element of volume (of the medium) and the surface S. The flux $Nt(1 - \Delta S/S)$ is distributed over the surface of the sphere; then, a flux $NRt(1 - \Delta S/S)$ is reemitted after reflection, and the output surface receives a fraction of it, $T\Delta S/(S - \Delta S)$. The real value of this fraction amounts to $NRTt\Delta S/S$, where T is the mean transmission coefficient corresponding to the passage of the light between two elements of the sphere's surface. We assume that the isotropy of the light flux is conserved after reflection; in other words, the output surface introduces only one negligible perturbation. In the second reflection, the flux uniformly distributed over the sphere is

$$NRTt\left(1 - \frac{\Delta S}{S}\right)\left(1 - \frac{\Delta S}{S - \Delta S}\right)$$

the fraction of the flux leaving through ΔS is $RT\Delta S(S - \Delta S)$.

Hence, the flux leaving by ΔS is

$$NR^2T^2t\,\frac{\Delta S}{S}\left(1 - \frac{\Delta S}{S - \Delta S}\right)$$

According to our hypotheses, the same fraction of the flux distributed over the sphere will leave on each reflection. From this, we find that the flux leaving on the n-th reflection is

$$NR^nT^nt\,\frac{\Delta S}{S}\left(1 - \frac{\Delta S}{S - \Delta S}\right)^{n-1}$$

The total number of photons leaving the surface S is thus /14

$$Nt\,\frac{\Delta S}{S}\left[1 + RT + R^2T^2\left(1 - \frac{\Delta S}{S - \Delta S}\right) + \ldots\right]$$

which is expressed as

$$n = Nt\,\frac{\Delta S}{S}\left[1 + \frac{RT}{1 - \left(1 - \frac{\Delta S}{S - \Delta S}\right)RT}\right]$$

or as

$$n = Nt\,\frac{\Delta S}{S}\left[\frac{1 + \left(\frac{\Delta S}{S - \Delta S}\right)RT}{1 - \left(1 - \frac{\Delta S}{S - \Delta S}\right)RT}\right]$$

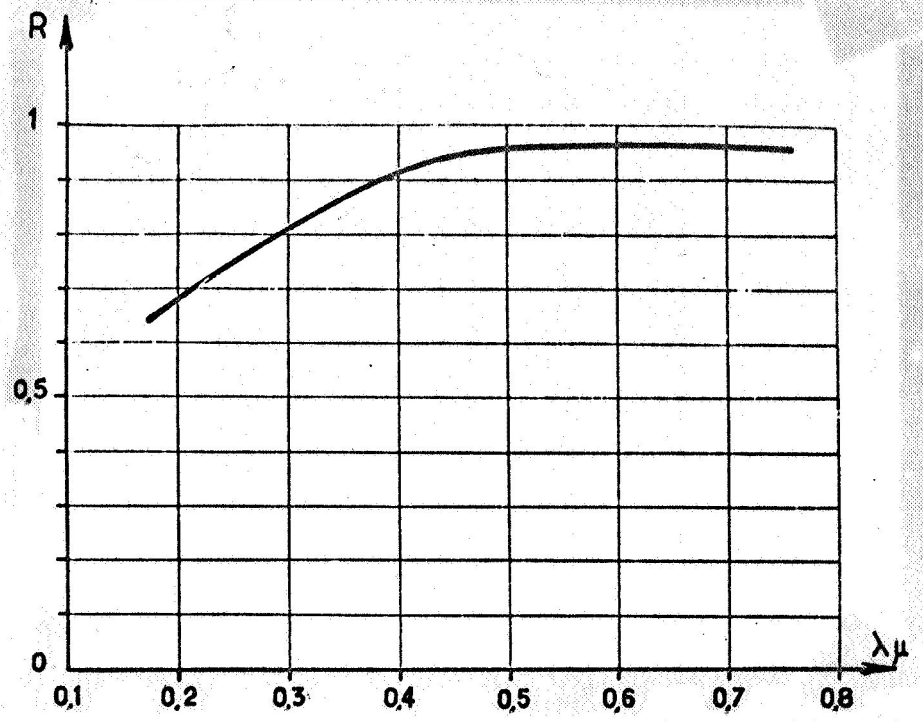

Figure 4. Reflection Coefficient R(λ).

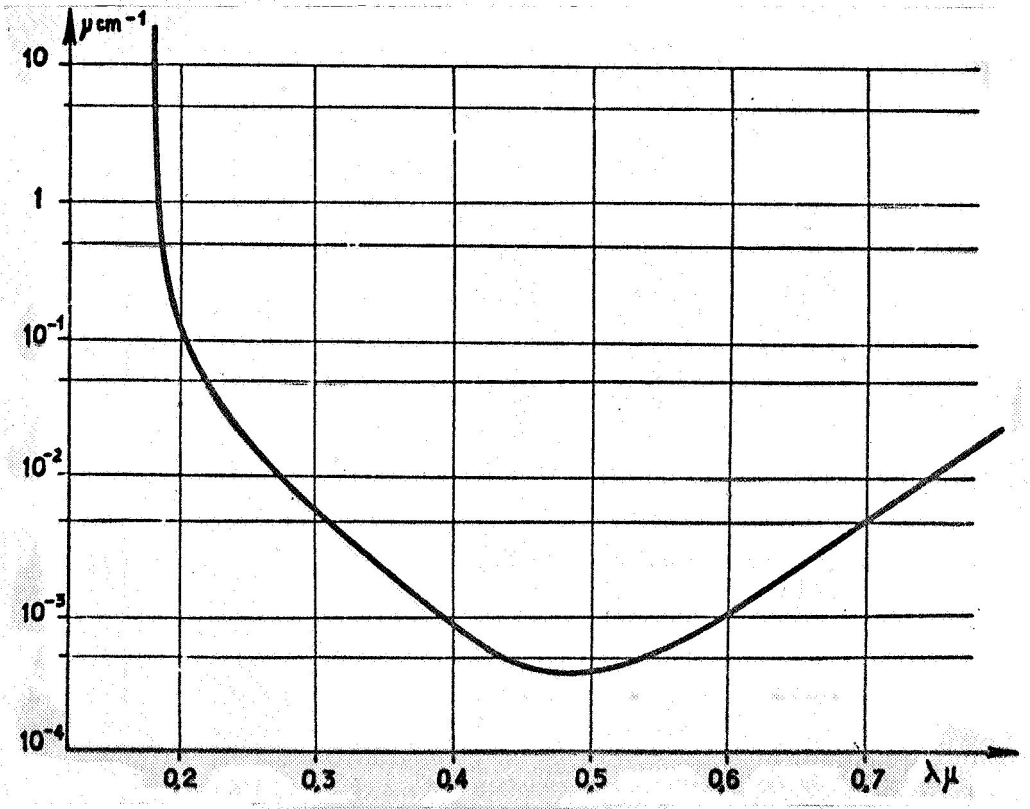

Figure 5. Absorption by Water.

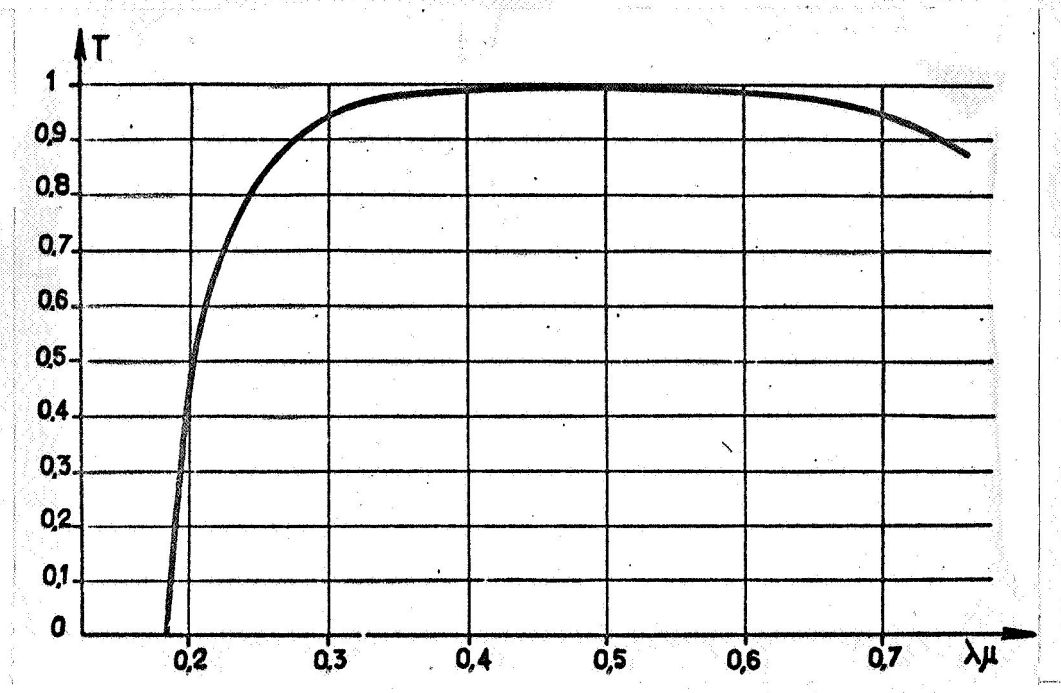

Figure 6. Transmission for a 9-cm Path.

The optical yield of the tank $\eta_0 = n/2N$ then takes the form:

$$\eta_0 = \frac{t.\ \Delta S}{2\ S}\left[\frac{1 + \left(\frac{\Delta S}{S - \Delta S}\right) RT}{1 - \left(1 - \frac{\Delta S}{S - \Delta S}\right) RT}\right]$$

b. The Mean Transmission Factor t Between an Emitter Element dv and the Surface S.

Let us consider the spectrum of the paths; i.e., the existence probability p(x) of a path between the element dv and the surface; the length of this path is between x and x + dx. Because of symmetry, it is sufficient to consider the ensemble of the rays emitted over the entire volume of the medium in a given direction.

The ensemble of the emitter points between the distances x and x + dx from the surface S' is situated between the two spheres S' and S'' derived from S by the translations $\vec{xu}$ and $(x + dx)\vec{u}$. Here, $\vec{u}$ is the unit vector in the direction considered (Fig. 7a).

The volume of element dv is $dv = \pi y^2 dx = \pi (r^2 - x^2/4)\, dx$, where y is the radius of the circle produced by intersection of spheres S and S'.

The spectrum of the paths is $p(x) = dv/Vdx = 3(r^2 - x^2/4)/4r^2$ (Fig. 8a). The mean path is $1_m = \int_0^{2r} x\, p(x)dx = 3r/4$.

The transmission factor for a path x is $e^{-\mu x}$. If each path has an existence probability of p(x), the mean transmission factor is written

$$t = \int_0^{2r} p(x)\ e^{-\mu x}\, dx$$

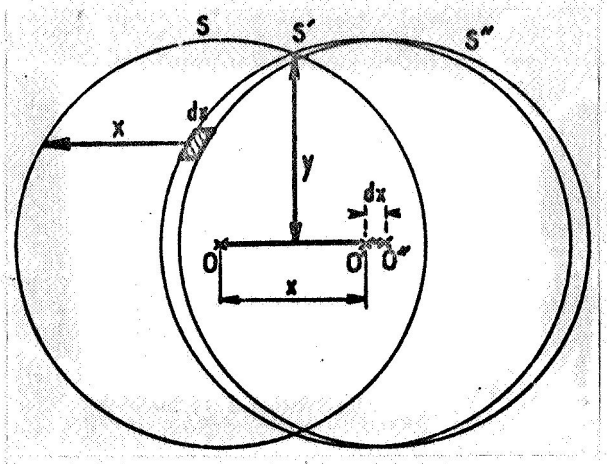

Figure 7a.

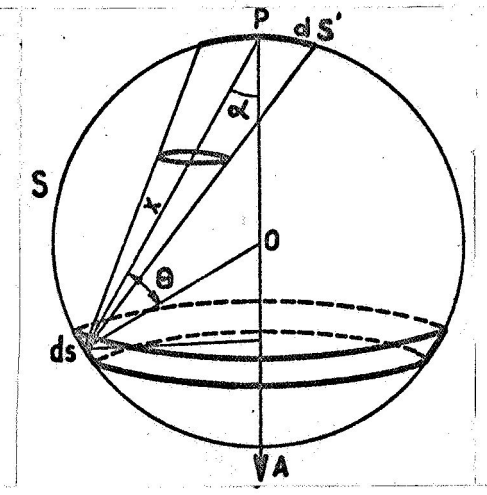

Figure 7b.

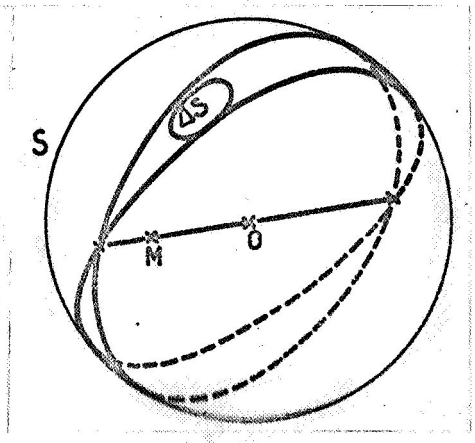

Figure 7c.

which amounts to

$$t = \frac{3}{2}\left[\frac{1}{2\mu r} - \frac{2}{(2\mu r)^2} + 2\left(\frac{1}{(2\mu r)^3} + \frac{1}{(2\mu r)^4}\right)e^{-2\mu r}\right]$$

For low values of μ (where $\lambda < 2500$ Å), the expression $e^{-2\mu r}$ can be expanded, and we get the approximate formula

. This formula is close $\exp\left(\frac{-3\mu r}{4}\right)$ or $\exp(-\mu l_0)$.

c. Mean Transmission Coefficient T Between two Reflections

Let us assume that the diffuse reflection obeys Lambert's law (Fig. 7b). The element ds sends the flux $d\Phi$ across dS', which receives the fraction $dp = d\Phi / \Phi$ of the total flux Φ. This Φ is found from Lambert's law to be $\Phi = \pi B\, dS'$. Then, dp is expressed by

$$\frac{d\Phi}{\Phi} = B\left(\frac{dS' \cos\theta \cdot dS \cos\theta}{x^2 \cdot \pi B\, dS'}\right) = \frac{dS}{S}$$

We choose the surface element dS shown in Fig. 7b . Then,

$$dp = \frac{dS}{S} = \frac{2x \cdot x \sin\theta \cdot 2r\, d\theta}{4\pi r^2} \quad \text{avec} \quad \begin{matrix} x = 2r\cos\theta \\ dx = 2r\sin\theta\, d\theta \end{matrix}$$

/16

from which,

$$dp = \frac{x\,dx}{2r^2} \text{ et } p(x) = \frac{dp}{dx} = \frac{x}{2r^2}$$

The average value of x is $L_0 = \int_0^{2r} x\, p(x)\, dx = \frac{4r}{3}$.

In the same way, the transmission factor/17 is calculated by

$$T = \int_0^{2r} p(x)\, e^{-\mu x}\, dx$$

which is the same as

$$T = 2\left[\frac{1}{(2\mu r)^2} - \left(\frac{1}{(2\mu r)^3} + \frac{1}{2\mu r}\right)e^{-2\mu r}\right]$$

For low μ values ($\lambda > 2500$ Å) we get

$$T \simeq 1 - \frac{4\mu r}{3} + \frac{4\mu^2 r^2}{3}$$

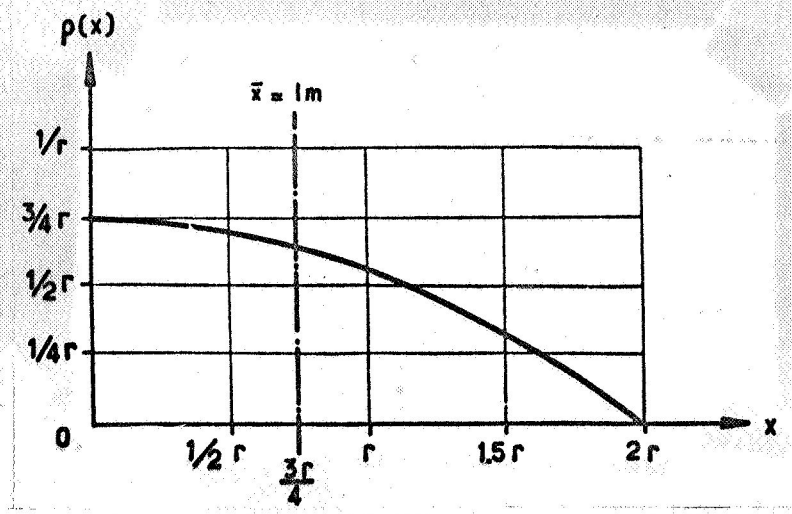

Figure 8a. Spectrum of the Paths between dv and S.

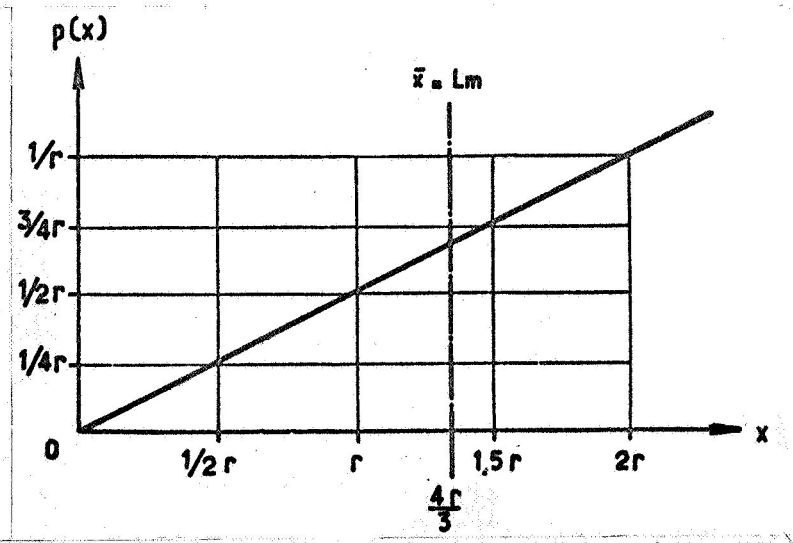

Figure 8b. Spectrum of the Paths between ΔS and S.

or

$$T = \exp(-\mu L_0)$$

d. Results and Discussion

In our experiment, the radius of the equivalent sphere is 6.5 cm and the paths l_0 and L_0 are, respectively, 5 and 9 cm. We have drawn a family of curves, under these conditions, which show the yield as a function of the absorption μ and of the coefficient of reflection R. The abscissae are also measured off in wavelengths (Figure 10).

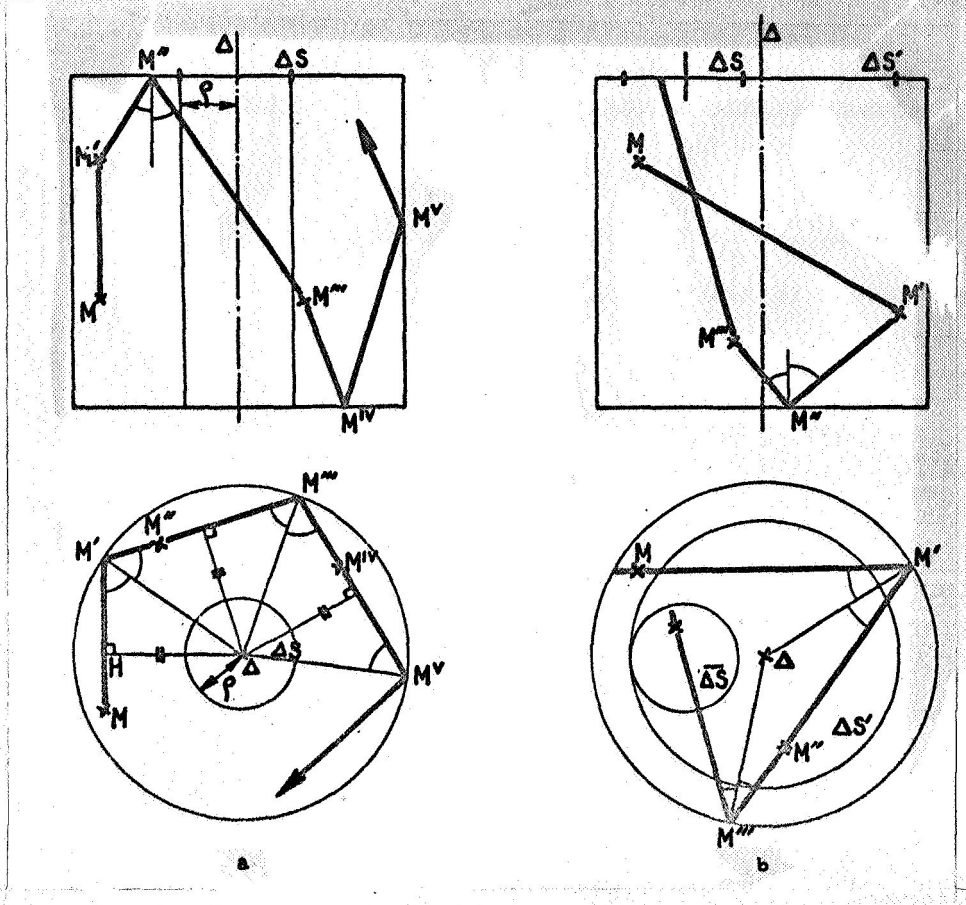

Figure 9. Effect of the Output Surface Location on the Collection of light in a Cylinder.

We can see that the yield shows very little variation for wavelengths between 4000 and 6000 Å, where the absorption of the water is weak. We note the considerable effect of the reflection factor since, for R = 0.9, the yield is only one-third of the maximum yield. We also note that the absorption μ has very little effect on the yield for poor reflections. The yield η_0 for R = 0 is $t\Delta S/2S$, and follows the variation of t with the wavelength.

We recall that the preceding calculations were made under the assumption that the walls were diffusive by reflecting. Indeed, it is theoretically impossible for ΔS to collect the entire flux emitted in the volume of a sphere with perfectly reflecting walls. A light ray always remains in the same incidence plane; for it to leave that plane, it is necessary that the plane cut the surface ΔS (Fig. 7c) of all the rays issuing from M, the only ones capable of leaving are those emitted between the two diametric planes tangent to the output surface. /19

In the case of our medium-containing vessel, that is, a cylinder, the problem is very similar provided the output surface ΔS is at the center of one of the bases. A ray emanating from M is reflected on the lateral surface at M' and on the base surface at M''. Each of the segments MM', M'M'', etc., always remains at the same distance

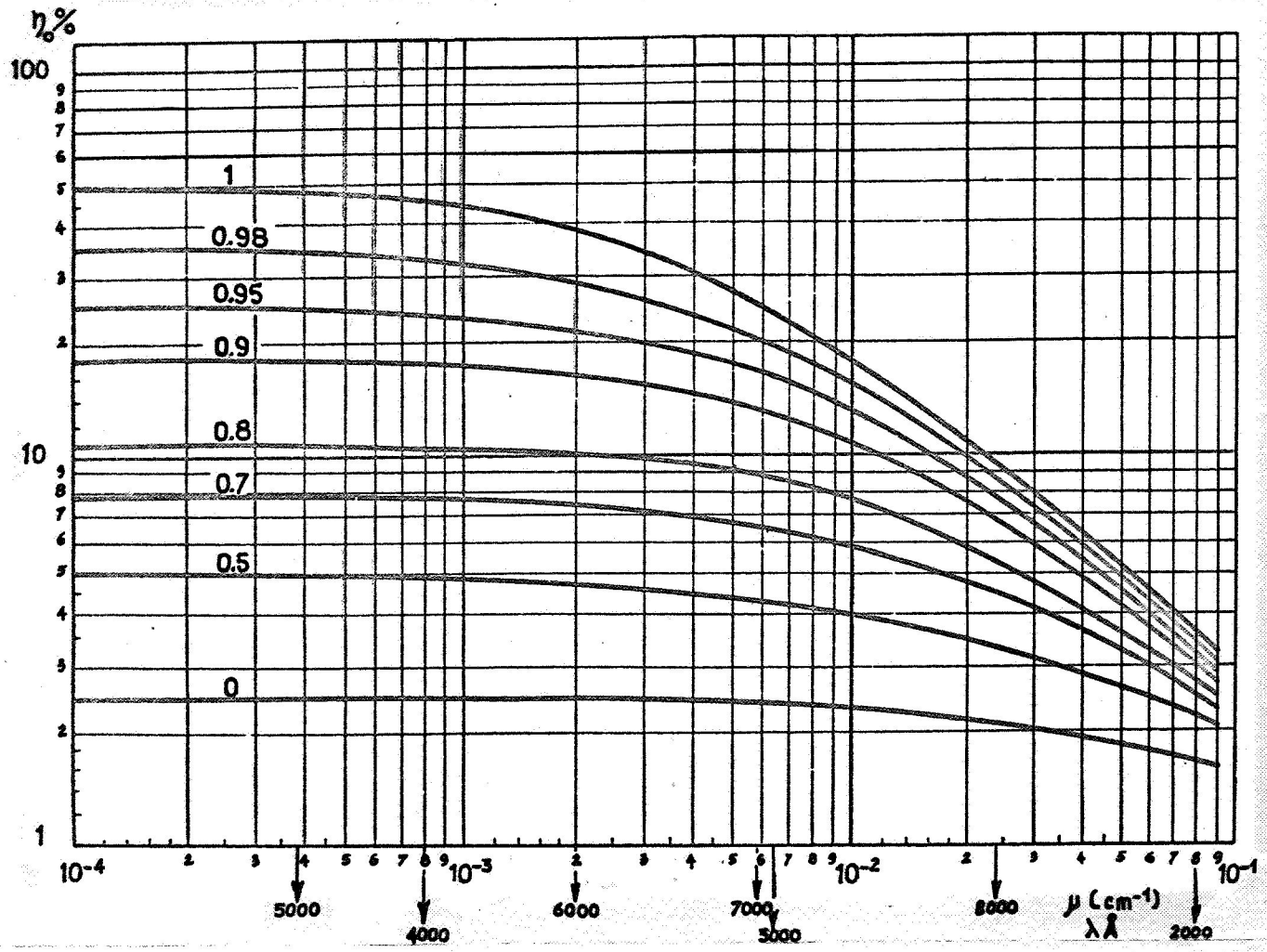

Figure 10. Optical Yield. The Abscissae are μ (the Absorption Coefficient per cm); the Parameter is R (the Reflection Coefficient).

from the axis Δ. For the ray to strike ΔS, this distance ΔH must be less than the radius s of the cylinder of ΔS (Fig. 9a).

To improve the yield, it is enough to offset the element ΔS. Indeed, the closer ΔS is to the periphery, the larger is the cylinder with base ΔS' and the volume of the emitter under consideration. This cylinder has the axis of Δ and is tangent to ΔS. A ray can leave through ΔS if it traverses this cylinder (Fig. 9b).

Thus it would seem that in an arrangement employing a coincidence measurement, where the photocathodes are of necessity eccentrically situated, the yield would not vary regardless of whether the material is diffusing or reflecting.

With the curves for the yield as a function of R (Fig. 10) taken into account, we must choose materials which are highly reflective for the short wavelength region.

We have evaluated the optical yield for each value of λ (Fig. 11). The maximum of 28% is obtained at 5300 Å, a wavelength for which the water absorption is only 9% after traversing 20 mean paths, and the reflection coefficient is 0.96.

The bandwidth at half the maximum is only 4000 Å; this is the luminous "selectivity" of the system.

4. Quantum Yield of the Photocathodes and the Number of Emitted Photoelectrons.

The photons are thus collected by each photocathode at a yield of $\eta_0(\lambda)$. If $\overline{C}(\lambda)$ is the Cerenkov emission spectrum (see § I. 1), their composite spectrum is $C(\lambda)$, $\eta_0(\lambda)$. The response $S(\lambda)$ of the photocathodes limits this spectrum in the vicinity of 0.65 μ. The total response of the system can be given by

$$\int S(\lambda)\, \overline{C}(\lambda)\, \eta_0(\lambda)\, d\lambda$$

The response of the cesium-antimony photocathodes is maximum in the blue range and extends into the ultraviolet. To take advantage of this part of the spectrum, we use quartz windows which permit attaining 0.2 μ without too much loss of light. We shall study two types of spectral response, AVP and UVP, for a high-gain photomultiplier.

The manufacturers give the curve of the photocathode sensitivity in mA/watt, i.e., in reality, the number of photoelectrons emitted per watt of incident light at a given frequency [9]. Indeed, the quantum yield is the ratio of the number of photoelectrons emitted to the number of incident photons, a number which is a function of the wavelength of the light. We express it as $\xi = \xi_0 S(\ )$ [10], where ξ_0 is a coefficient depending on the photocathode and $S(\lambda)$ is a function less than one which approaches zero for AVP at wavelengths less than 0.30 μ. This function is derived from the sensitivity in mA/watt by the following transformation:

$$\frac{dN_{phs}}{dN_{\nu}} = \frac{dN_{phe}}{dW} \times \frac{dW}{dN_{\nu}} = \frac{dN_{phe}}{dW} \times \frac{hc}{\lambda}$$

a relation which shifts the curve toward the ultraviolet region (Fig. 12). It can also be asserted that, for the UVP photomultiplier, the cutoff at 0.2 μ depends essentially on the thickness of the quartz window used; the transmission factor of the water is low at this wavelength and the yield is also low.

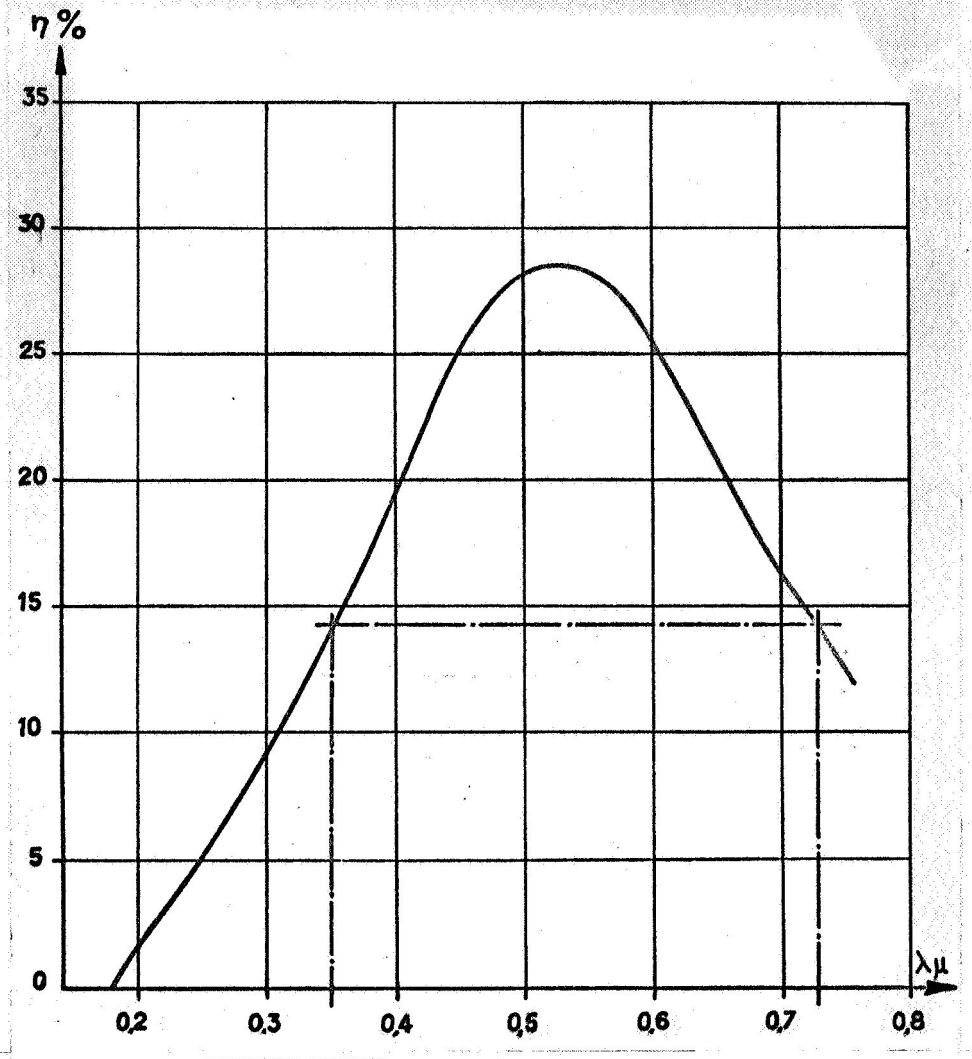

Figure 11. Optical Yield $\eta_0(\lambda)$.

At the maximum response, one has

$$\xi_0 = 11\% \text{ for AVP,}$$
$$\xi_0 = 13.5\% \text{ for UVP}$$

a. Response to Emitted Radiation per Centimeter of the Electron Path

We have seen, in § I. 2, that the number of photons emitted per unit length of the electron path was

$$\frac{dN_\nu}{dl} = \frac{2\pi}{137}\int\left[1 - \frac{1}{\beta^2 n^2(\lambda)}\right]\frac{d\lambda}{\lambda^2}$$

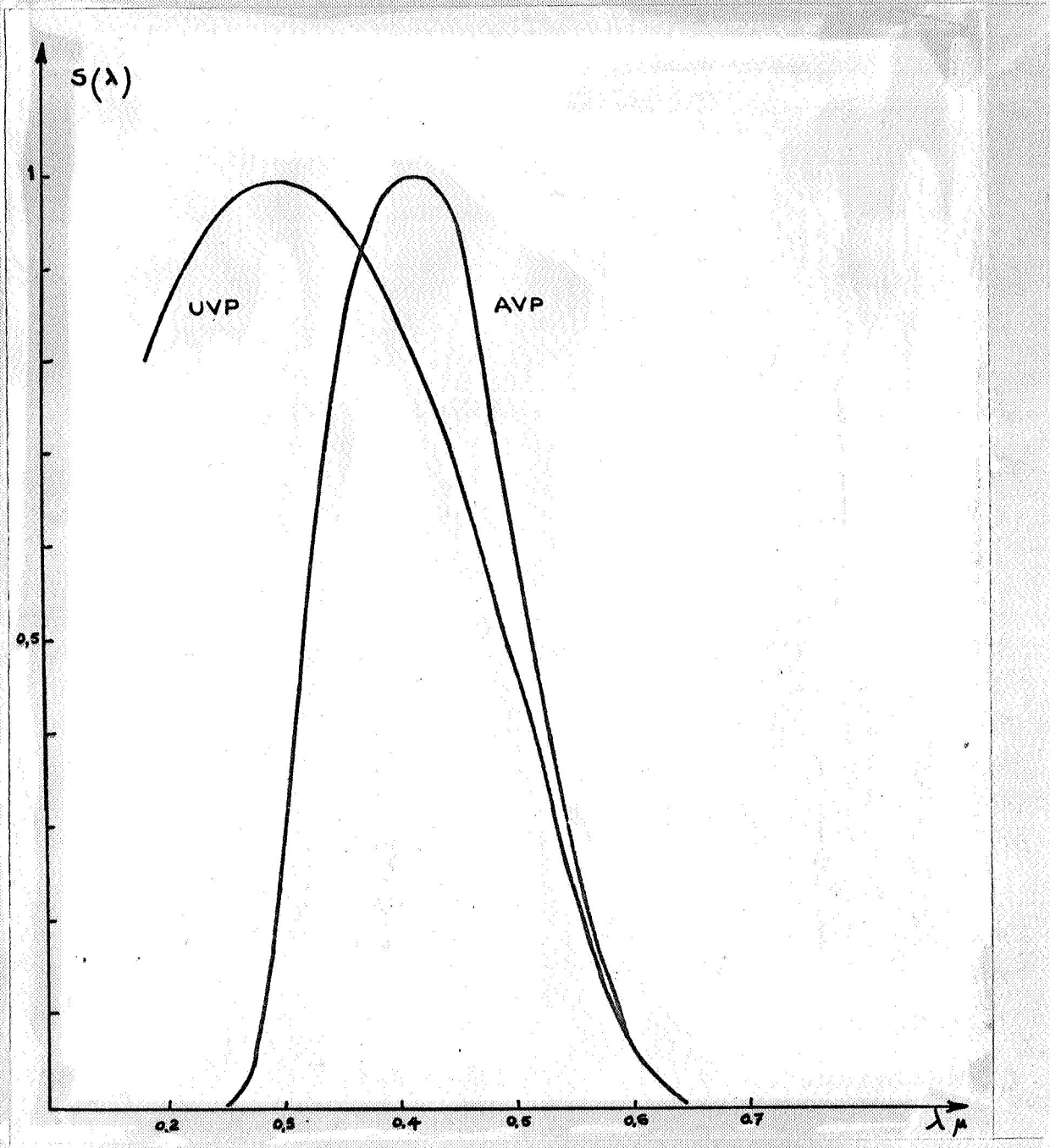

Figure 12. Spectral Response S(λ) of the Photocathodes.

If we ignore the random way in which the quanta yield their energy to the photoelectrons, we get, per unit length dl:

$$\frac{dN_{pae}}{dl} = \frac{2\pi\xi_0}{137}\int \left[1 - \frac{1}{\beta^2 n^2(\lambda)}\right] \frac{\eta_0(\lambda)\ S\ (\lambda)}{\lambda^3}\ d\lambda$$

that is, the number of photoelectrons ejected into the accelerating field of the photomultiplier optical input. /21

The variation in the index of refraction η for water does not exceed 1% between 0.65 μ and 0.45 μ, and reaches 15% only at 0.2 μ, where the optical yield $\eta_0(\lambda)$ becomes very low (2%). In the first approximation, then, we consider the expression $(1 - 1/\beta^2 n^2)$ independent of λ.

We then get /22

$$\frac{dN_{ph^e}}{dl} = \frac{2\pi\xi_e}{137}\left(1 - \frac{1}{\beta^2 n}\right)\int \frac{S(\lambda)\,\eta_0(\lambda)\,d\lambda}{\lambda^2} = B\left(1 - \frac{1}{\beta^2 n^2}\right)$$

Figure 13 shows the two curves for the composite response $\frac{S(\lambda)\,\eta_0(\lambda)\,\xi_e}{\lambda^2}$ for the AVP and UVP photomultiplier, respectively, the areas under the curves representing the coefficient B reduced by the factor of $2\pi/137$ of the relation above.

We thus find that: /23

$$B_{AVP} = 12 \text{ cm}^{-1}$$

$$B_{UVP} = 18 \text{ cm}^{-1}$$

This means that the UVP photocathode emits one and a half times as many electrons as the AVP photocathode, with a greater detection probability as well as greater output pulse amplitudes.

b. Computing the Number of Photoelectrons Emitted per Beta Ray of Given Energy.

We have just discussed the effect of various collection factors and have shown their influence on the number of photoelectrons emitted per centimeter of the path. We shall now consider the path-to-energy relation of beta rays.

The beta electron is emitted with an energy E and then slows down over its path, primarily because of ionization. At energies of the MeV order, the bremsstrahlung is virtually negligible. The critical energy for water, that is, the energy level above which the energy loss via bremsstrahlung is higher than the energy loss via ionization, is 93 MeV in the case of the electron [11].

In the course of the deceleration, Cerenkov light photons are radiated as long as the energy remains above the emission threshold of 260 keV. On the curve of the electron paths in water (Fig. 14), we note that the maximum paths are in the neighborhood of 10 mm. Thus, it is certain that all the beta rays are nascent and decay within the detector.

If x_1 is the abscissa of the electron origin and x_0 is the abscissa at which the electron has a kinetic energy equal to the Cerenkov threshold, the number of photoelectrons emitted by the photocathode will be

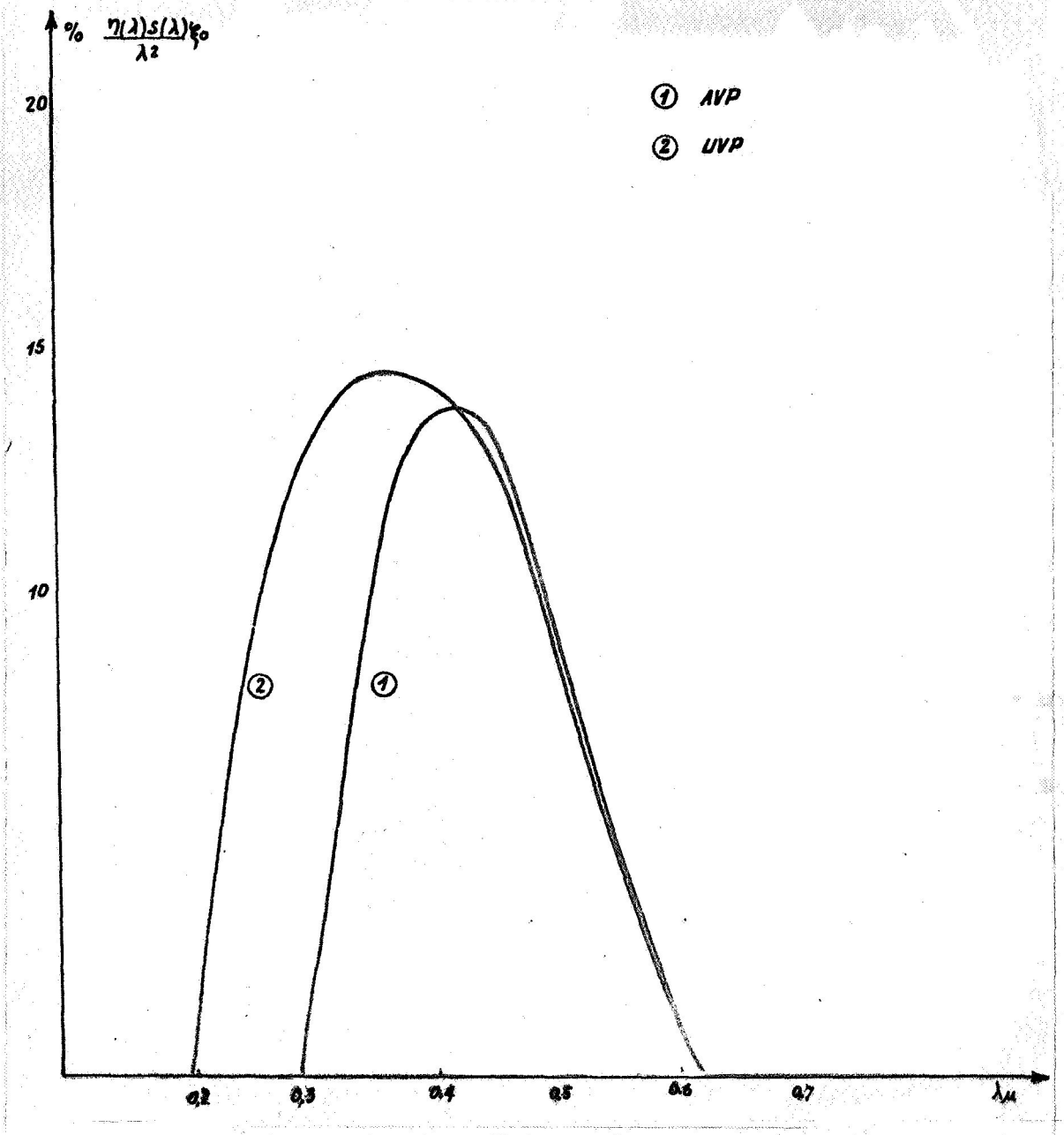

Figure 13. Overall Spectral Responses.

$$N_{phe} = B\int_{\lambda_1}^{\lambda_0}\left(1 - \frac{1}{\beta^2 n^2}\right) d\lambda$$

Since the velocity and the kinetic energy are functions of the path length, we can write this relation in terms of energy by changing variables [11]:

$$N_{phe} = B\int_{E_1}^{E_0}\left[1 - \frac{(E + m_0c^2)^2}{(E + 2m_0c^2)\,En^2}\right]\frac{d\lambda}{dE}\,dE$$

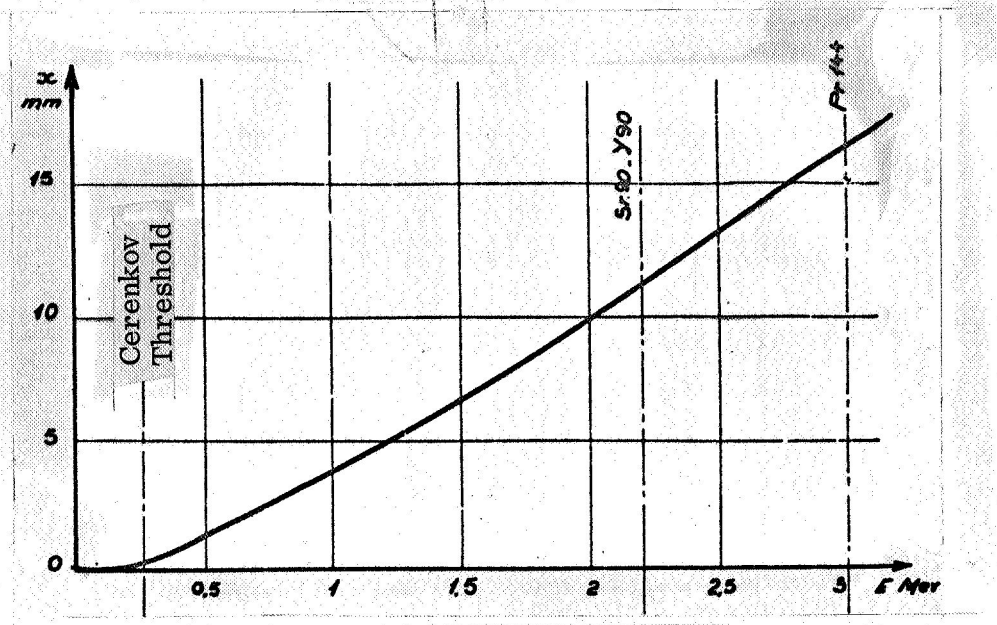

Figure 14. Beta Paths in Water.

/24

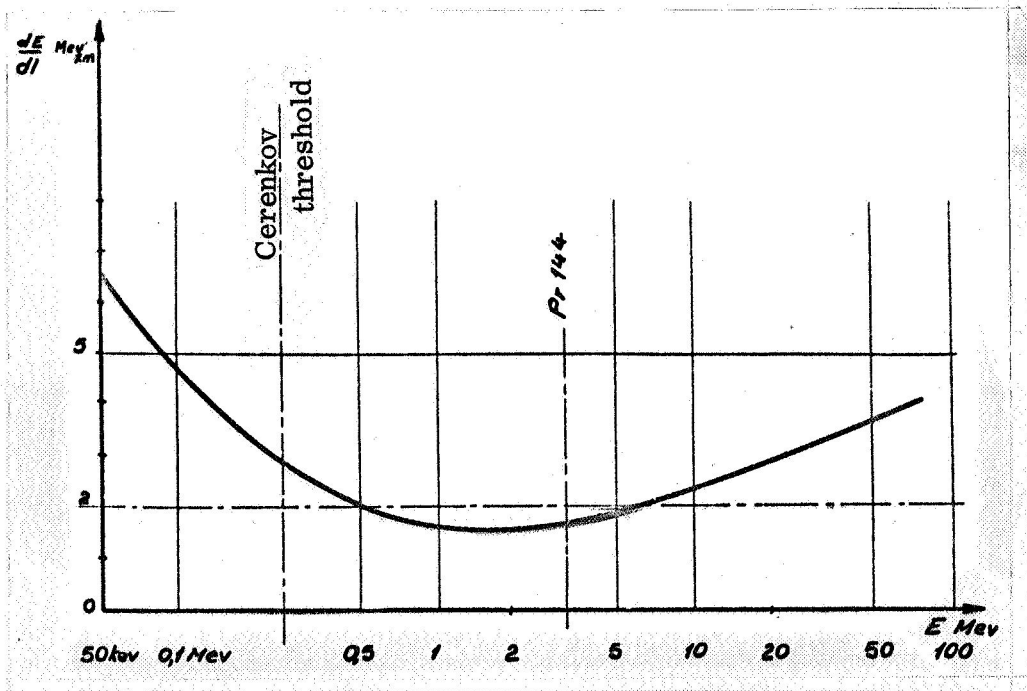

Figure 15. Energy Loss of a Beta Ray in Water.

where dE/dl is the particle energy loss by ionization shown in Fig. 15. This curve passes through a very shallow minimum in the energy band that interests us [12, 13]. We can arrive at a good approximation by considering that the energy loss per unit length dE/dl is constant and equal to 2 MeV/cm for water. The foregoing expression, when integrated, yields

$$N_{phe} = \frac{B}{2}\left[(E-E_0) - \frac{1}{n^2}(E-E_0) + \frac{m_0c^2}{2} \cdot \mathrm{Log}\left(\frac{E}{E_0} \cdot \frac{E_0 + 2m_0c^2}{E + 2m_0c^2}\right)\right]$$

For the two values of B given earlier and the following specified data

$$n = 1.34$$

$$E_0 = 0.26 \text{ MeV}$$

$$m_0c^2 = 0.51 \text{ MeV}$$

we can draw the curves for the average number of generated photoelectrons. In particular, we can see that in order to generate more than one photoelectron, on the average, we must have energy greater than 0.75 MeV for the UVP photomultiplier and 0.90 for the AVP photomultiplier (Fig. 16). These curves increase almost linearly at energies greater than one MeV, but saturation is attained when the energy of the electrons is sufficient for passage across and out of the vessel containing the medium. The number of emitted photoelectrons is then

$$N_{max} = B\int_0^1 \left(1 - \frac{1}{n^2}\right)$$

which amounts to 50 photoelectrons for the AVP and 75 for the UVP.

The curves $N_{phe} = f(E)$ are continuous and correspond only to the average number of photoelectrons. Discontinuous photoemission is produced in a random manner; it should be remembered that the curves given above really represent the number of "useful" Cerenkov photons multiplied by the average quantum yield ξ_0 of the photocathode.

5. Probability of Radiation Detection. /26*

We choose the Poisson law as the distribution function of the number of photoelectrons [14]. P(x) is the probability of detecting x photoelectrons when N photoelectrons exist on the average, and is expressed as

$$P_N(x) = \frac{e^{-N} N^x}{x}$$

We note that the probability of having no photoelectron emitted is low only for an average of four emitted electrons. The probability of emission of one photoelectron is 0.37 for an average of one electron.

If the discrimination threshold is such that any pulse corresponding to a single photoelectron is counted, the detection yield of the equipment will be the probability of collecting at least one photoelectron for some number N_{phe} emitted on the average; i.e.,

$$P_d = 1 - P_N(o) = 1 - e^{-N}$$

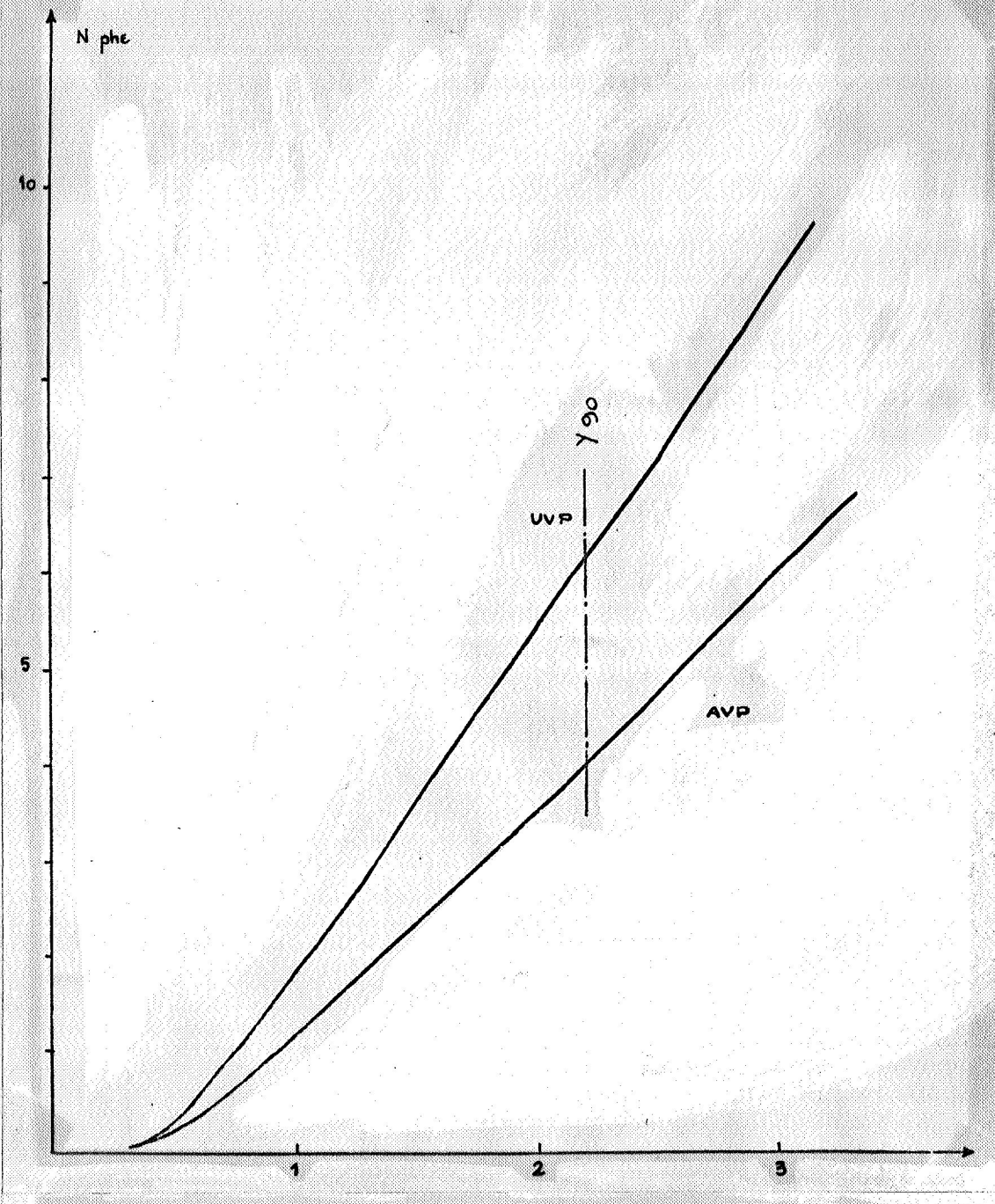

Figure 16. The Number of Emitted Photoelectrons.

The number N_{phe} enters each of the relations considered in connection with the energy level E for the beta ray. We can therefore assign a detection probability of $p_d(E)$ (Fig. 17) to each beta ray of energy E.

The detection occurs at 50% for energy levels greater than 0.7 MeV, and at practically 100% for energy levels above 2 MeV.

6. Detection of Strontium in Water

a. Spectrum of Beta Decay.

Emission of beta radiation occurs in the course of the reaction

$$\text{or:}\quad \begin{matrix}\text{Neutron} \longrightarrow \text{proton} + \beta^- + \text{neutrino}\\ \text{Proton} \longrightarrow \text{Neutron} + \beta^+ + \text{neutrino}\end{matrix}$$

There is therefore a change of one unit in the atomic number.

Thus:

$$Sr^{38}_{90} \longrightarrow Y^{39}_{90} \longrightarrow Zr^{40}_{90}$$

The beta electrons are emitted with an energy distribution from 0 to a maximum value E_{max}. The form of the spectrum is characteristic of the reaction, and does not vary with the age of the source [15, 16].

The detector permits analysis of water polluted by beta emitters as long as the maximum energy E_{max} of the spectrum is above the Cerenkov threshold of 260 keV (to keep the detection probability from being zero). In the case of strontium 90, the emission is doubled. Strontium decays with a period of 24 years, emitting electrons of 0.65 MeV maximum energy; its daughter product, yttrium 90, has a decay period much shorter than its parent (64 hours), with a maximum spectral energy at 2.2 MeV.

Because of the large ratio between these periods, the activity of the two species at any instant are identical and equal to $\frac{A_0}{\tau_a} e^{-t/\tau_a}$, where A_0 is the number of strontium atoms present at zero time, τ_a is the decay time constant, and A_0/τ_a is the activity at zero time.

The energy spectrum has been mapped out here by taking a band dE of 100 keV. That is to say, p(E) is the probability of emission of a beta particle with an energy between E and E + 100 keV.

The normalization condition is written as

$$\int_0^{E_{max}} p(E)\, dE = 1 \quad \text{(figure 18).}$$

b. Probability of Beta Detection in the Spectrum

Any energy of a beta ray corresponds to some number of emitted photoelectrons and consequently a certain coincidence detection probability p_d^2. The probability of observing a disintegration at an energy E is /28

$$P = P_d^2\, P(E) \text{ (figure 19).}$$

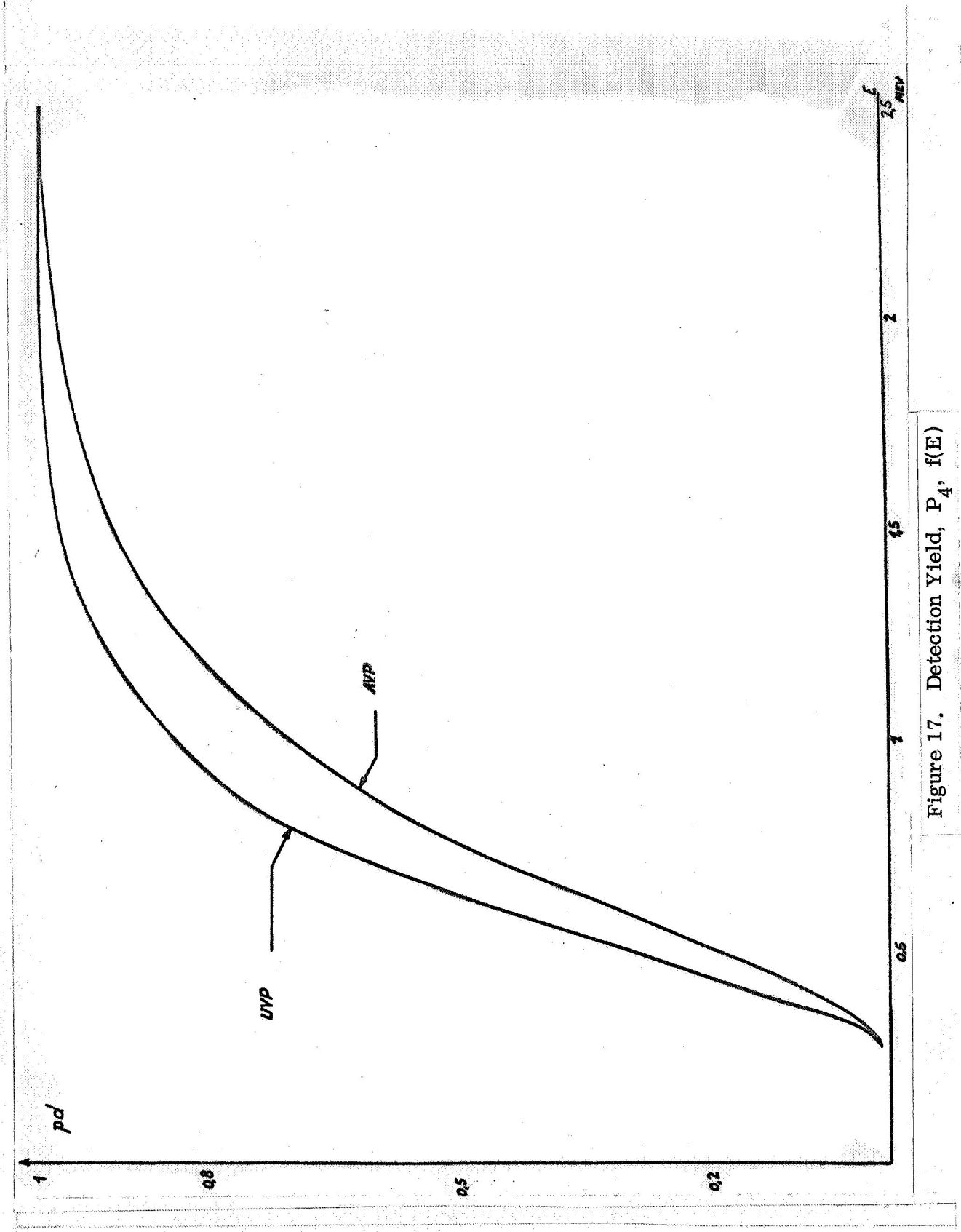

Figure 17. Detection Yield, P_4, f(E)

c. Yield of the Equipment

The probability of observing any beta ray of the spectrum expresses the yield, and is written

$$\eta = \int_{0,25}^{E_{max}} p_i \, p(E) \, dE$$

The pulses arrive in coincidence at the two photomultipliers in contact with the water. The coincidence count yield is η (see § I. 3), and if A is the activity of the water expressed in dpm/liter, the counting rate obtained is $N_s = A \eta$.

We thus find that

$$\eta_{AVP} = 0.20$$

$$\eta_{UVP} = 0.26$$

which means that, for an acitivity of $5 .10^{-7}$ μc/cc (1100 dpm/l) the count with the AVP is 220 cpm, while with the UVP it is 290 cpm.

The use of a perfect reflector (R = 1) would give 330 cpm and 410 cpm for the AVP and the UVP, respectively.

7. Application to the Detection of Gamma Radiation

It is interesting to evaluate the gamma yield of the detector, first, for the possible dosage of gamma emitters in the water, and second, to evaluate the action of sources close to gamma rays, particularly the ambient radiation.

We shall return to the preceding case after determining the probability of producing an electron with the kinetic energy E by means of a gamma ray.

Three processes are possible:

a) the photoelectric effect;
b) the Compton effect;
c) the effect of pair generation.

Examination of the cross section curves shows that the photoelectric effect is especially high at energies which are too low for the Cerenkov effect to occur. The probability of existence of the materialization effect is very low in water up to about ten MeV [16].

For energies of the order of one MeV the most important is the Compton effect. For Colbalt 60, whose highest gamma energy is 1.3 MeV, an electron is emitted with energy E which varies with the direction of the diffused photon as

$$E = h\nu_0 \frac{\alpha (1 - \cos \theta)}{1 + \alpha (1 - \cos \theta)} \quad \text{with } h\nu_0 = 1,3 \text{ MeV (Cobalt 60).}$$

$$\alpha = \frac{h\nu_0}{m_e c^2}$$

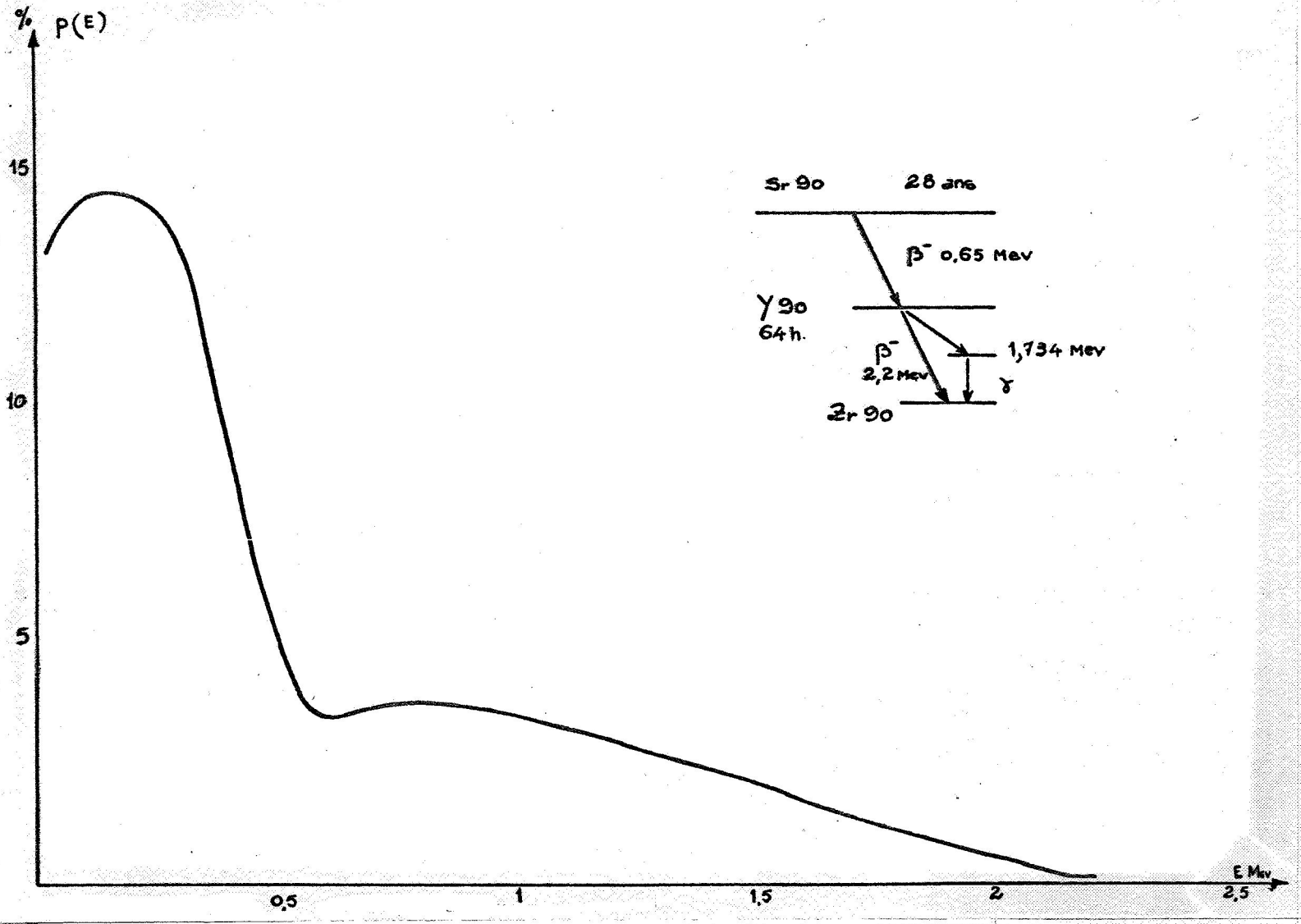

Figure 18. The Sr90-Y90 Spectrum (dE = 100 keV band).

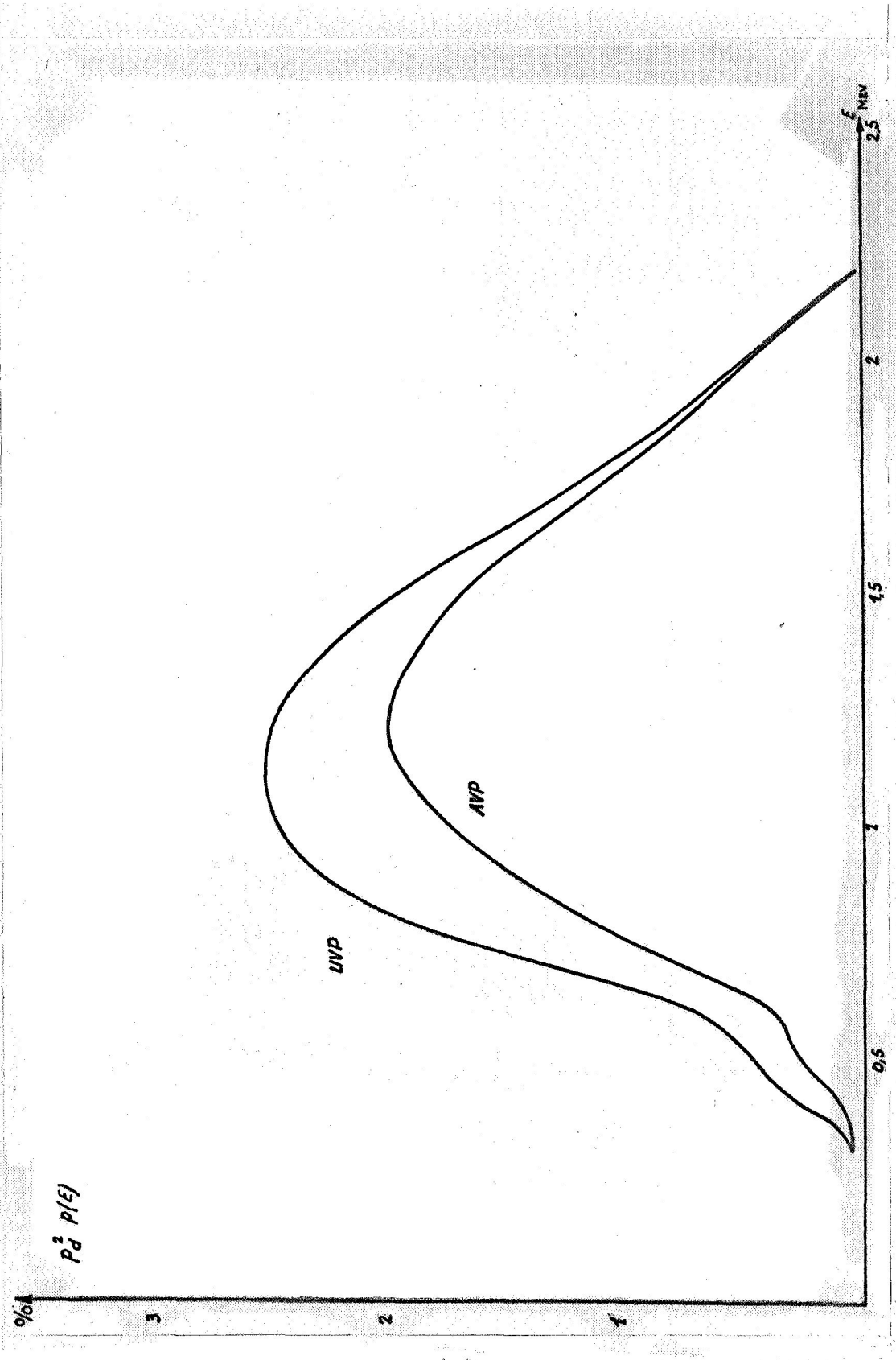

Figure 19. Probability of Observing a Beta Particle of Energy E in Coincidence.

The maximum energy of the electron is

$$\frac{h\nu_0}{1+\frac{1}{2\alpha}}$$

that is, practically 1.1 MeV.

The energy spectrum of Compton electrons is favored at the energies close to the maximum. Hence, one can foresee that the detection yield for electrons will be good. (see Fig. 21). /31

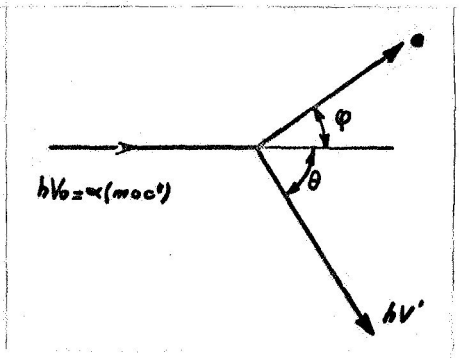

Figure 20. The Compton Effect.

However, every gamma ray is not absorbed in the medium. The curves for the cross section [16] show that for energies of the order of one MeV, the total absorption cross section for the Compton effect is of the order of 0.03 cm^2/g. For water and for a mean path of 8 cm, the number of absorbed gamma rays is $1 - e^{-\mu x}$, and only a fifth of the total radiation can give rise to a Compton-spectrum electron. Thus the probability p_c of this electron having an energy of E is added to the detection probability discussed in § I. 5.

The detection yield is therefore

$$\eta = \int_{0.25}^{E_{max}} p\, p_c^1\, dE.$$

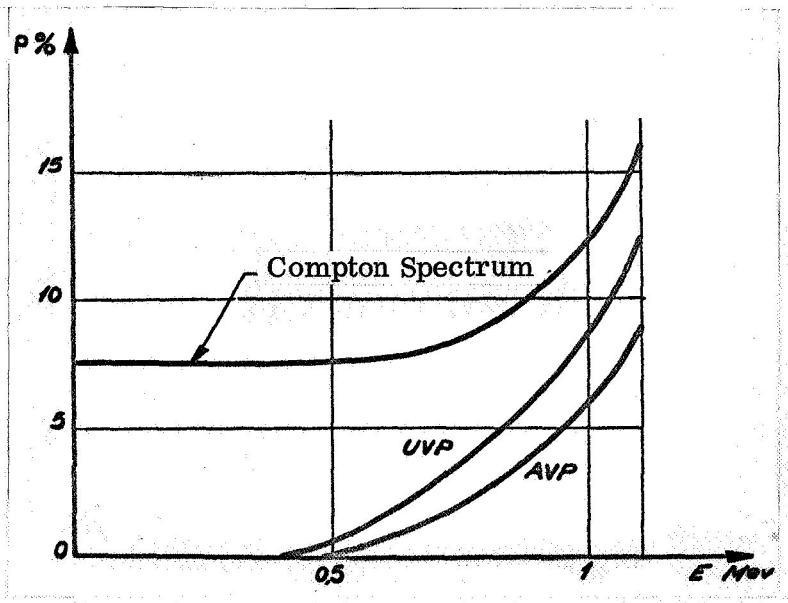

Figure 21. Detection Probability for a Compton Electron.

Thus, if we place a solid Co^{60} source at the bottom of the tank, the useful radiation /32
is within a solid angle of about 2π ; and, if A is the activity of this source and the radiation absorbed is one-tenth of the emitted radiation, the counting rate is $N_s = \frac{A\eta}{10}$.

For cobalt,

$$\eta_{AVP} = 25\ \%$$

$$\eta_{UVP} = 37\ \%.$$

For a source of $20\ \mu c$, these yield values involve counting rates of 1,000,000 and 1,500,000 cpm, respectively.

In the same way, the ambient gamma radiation produces a counting rate in the neighborhood of $A\eta/5$, where A is the number of gamma rays passing through the water per unit time.

8. Pulse Levels

All the signal pulses correspond to at least one emitted photoelectron. The pulse height is thus a function of the number of electrons emitted by the photocathode at the same time. If p(1) is the probability of collecting a single photoelectron, we can estimate the probability of obtaining at least two photoelectrons:

$$P = 1 - p(0) - p(1) = 1 - e^{-N}(1 + N)$$

Because of the introduction of N, this relation is a function of the energy of the emitted beta ray.

By the processes utilized in § I. 5, that is by multiplying this probability by the existence probability of a beta ray in the strontium-yttrium spectrum, we determine the probability of a cathode emitting at least two photoelectrons:

$$\eta_1 = \int_{0,28}^{E_{max}} P.\ p(E)\ dE$$

In this way, we get 16% for the AVP photomultiplier, and 22% for the UVP. The difference between the photomultipliers is much more appreciable with respect to pulse height than with respect to the number of pulses.

One can also determine the average number of photoelectrons emitted over the entire spectrum. If N(E) is the number of electrons incident on the multiplier, and if p(E) is the existence probability, the average value is expressed by

$$\bar{n} = \int_{0,28}^{E_{max}} N(E)\ p(E)\ dE$$

which gives 0.7 photoelectrons for the AVP and 1.1 photoelectrons for the UVP.

Of course, these quantities should be only considered as mathematical averages, since the output pulse corresponds only to discrete values of charge.

We can thus say that the detection probability is appreciably improved by using photomultipliers with quartz windows, but especially that the pulse amplitude has risen by 60%.

9. Shape of the Light Pulse

Because of the small number of emitted photoelectrons, often limited to just one, the shape of the voltage pulse at the photomultiplier anode depends only slightly on the light collected by the photocathode. We can, nevertheless, determine the collection time of the photons, particularly in the case of cosmic radiation which can furnish a large quantity of illumination.

The emission time is very short since it corresponds to the lifetime of the beta ray in water. At a maximum, this time is of the order of $3 \cdot 10^{-11}$ sec. Cosmic rays, on the other hand, traverse the entire tank and induce light emission during a period of $3 \cdot 10^{-10}$ sec. This is a very short time, but the time of collection of all the photons emitted by a disintegration is much larger. Of these, some are collected directly by the photocathode and constitute the beginning of the pulse, which continues as long as the photons keep arriving after several successive reflections. /33

We know the general expression for the optical yield:

$$\eta_0 = \frac{\Delta S}{2S} t \left[1 + \sum_1^{\infty} R^n T^n \left(1 - \frac{\Delta S}{S - \Delta S}\right)^{n-1}\right]$$

The series converges, and the term $\frac{\Delta S}{2S}$ is the pulse height which is independent of the coefficient of reflection and the number of reflections. The pulse then drops off in accordance with

$$R^n T^n \left(1 - \frac{\Delta S}{S - \Delta S}\right)^{n-1}$$

We can determine, for each wavelength, the number of required reflections for a collection of 90 % of the reflected light; i. e., we determine the threshold n at which the expression

$$\frac{\sum_{n+1}^{\infty} R^n T^n \left(1 - \frac{\Delta S}{S - \Delta S}\right)^{n-1}}{\sum_1^{\infty} R^n T^n \left(1 - \frac{\Delta S}{S - \Delta S}\right)^{n-1}}$$

is less than 10 %, or

$$R^n T^n \left(1 - \frac{\Delta S}{S - \Delta S}\right)^n < 10 \text{ p. } 100$$

from which,

$$n > \frac{-1}{\log \left(1 - \frac{\Delta S}{S - \Delta S}\right) + \log RT}$$

Assuming perfect transmission ($\mu = 0$), we have determined the number of required reflections and the theoretical pulse rate for different values of R (Figs. 22 and 23).

Each reflection corresponds to a path of $4r/3$. For n reflections, the duration of a pulse is

$$\tau = \frac{4\ nr}{3\ v}$$

if v is the velocity of light in the medium. Then $\tau = 4 \cdot 10^{-10}$ n seconds.

We have drawn the two curves for $-\tau = f(\lambda)$, the duration of the light pulse (Fig. 24) and $-\frac{\eta_0(\lambda)}{\lambda^2}$, the spectrum of the light pulse (Fig. 25).

We see that, in the wavelength range of 0.4 to 0.6 μ, the pulse length varies only slightly and corresponds to about twenty reflections, the spectral maximum being precisely at 0.4 μ.

In the preceding calculation, we assumed that the photons arrive in successive packets, and that all photons corresponding to the n-th reflection arrive at the same time after those of the (n-1)th reflection. This is obviously not the case in reality, in which a photon which has undergone n reflections may arrive before a photon which leaves directly.

The light pulse is not sufficient to define the voltage pulse because several factors are equally involved; these are the spectral response of the photocathodes, the anode time constant, the random manner with which the multiplication and the photoemission occur. We should, however, bear in mind that the signal level of approximately a single photoelectron emitted is about the same as for a packet of photons.

/34

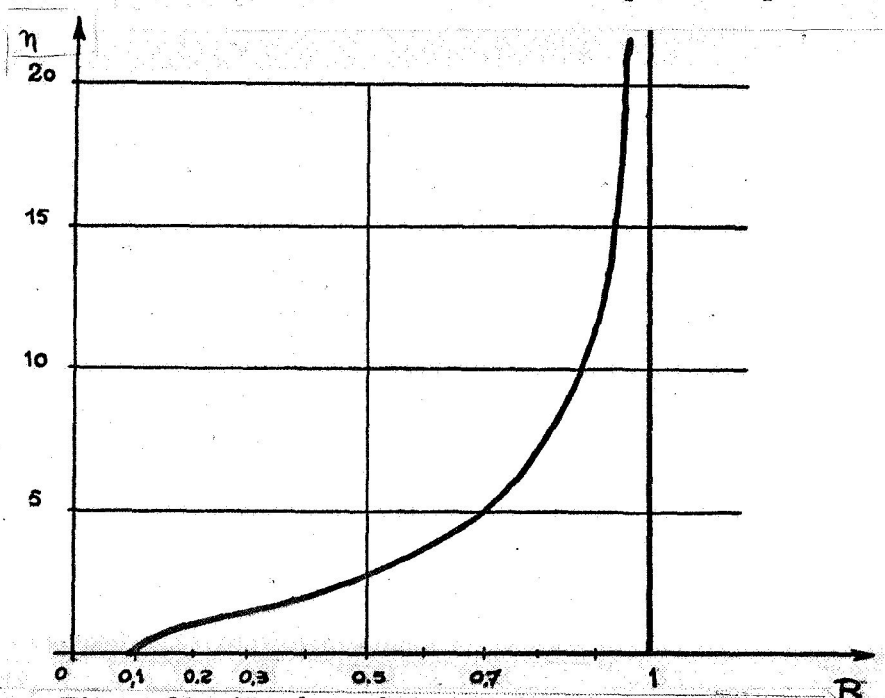

Figure 22. Number of Required Reflections ($\mu = 0$)

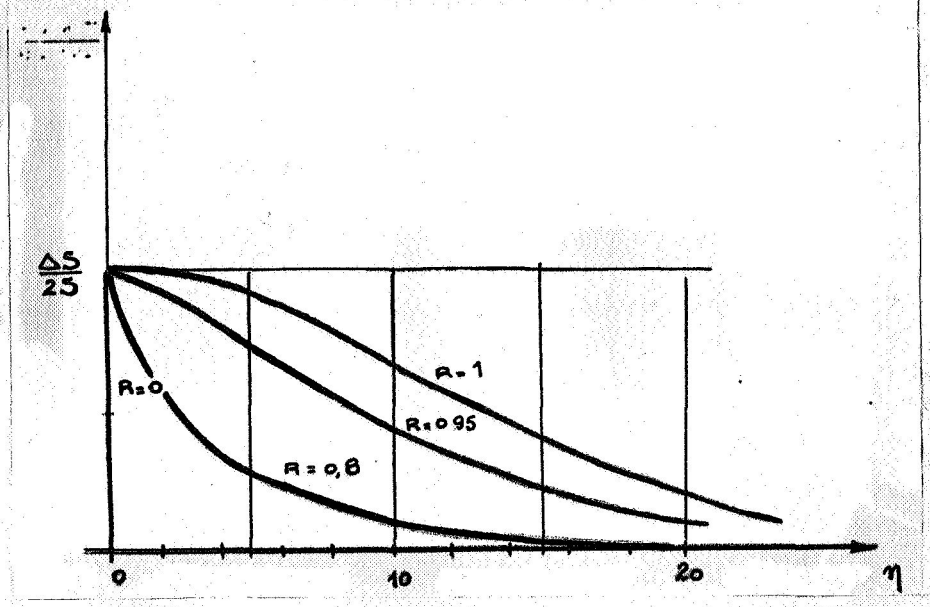

Figure 23. Pulse Rate for $\mu = 0$.

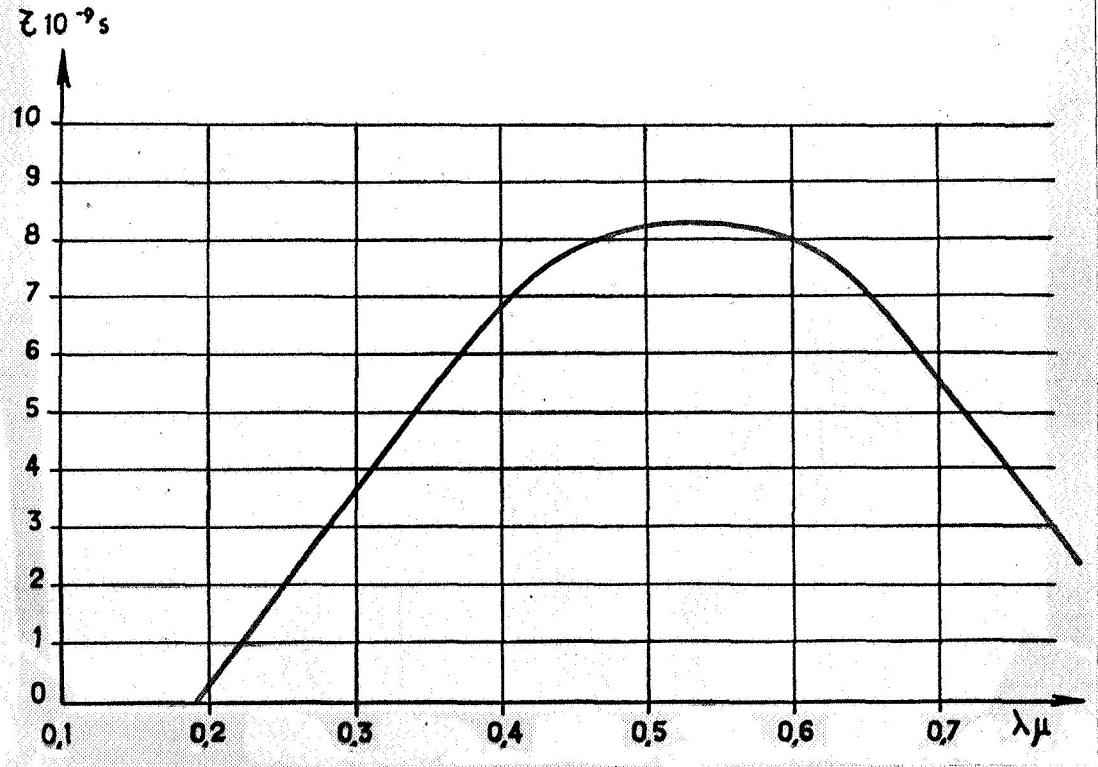

/35

Figure 24. Duration of Light Pulse Due to Multiple Reflections.

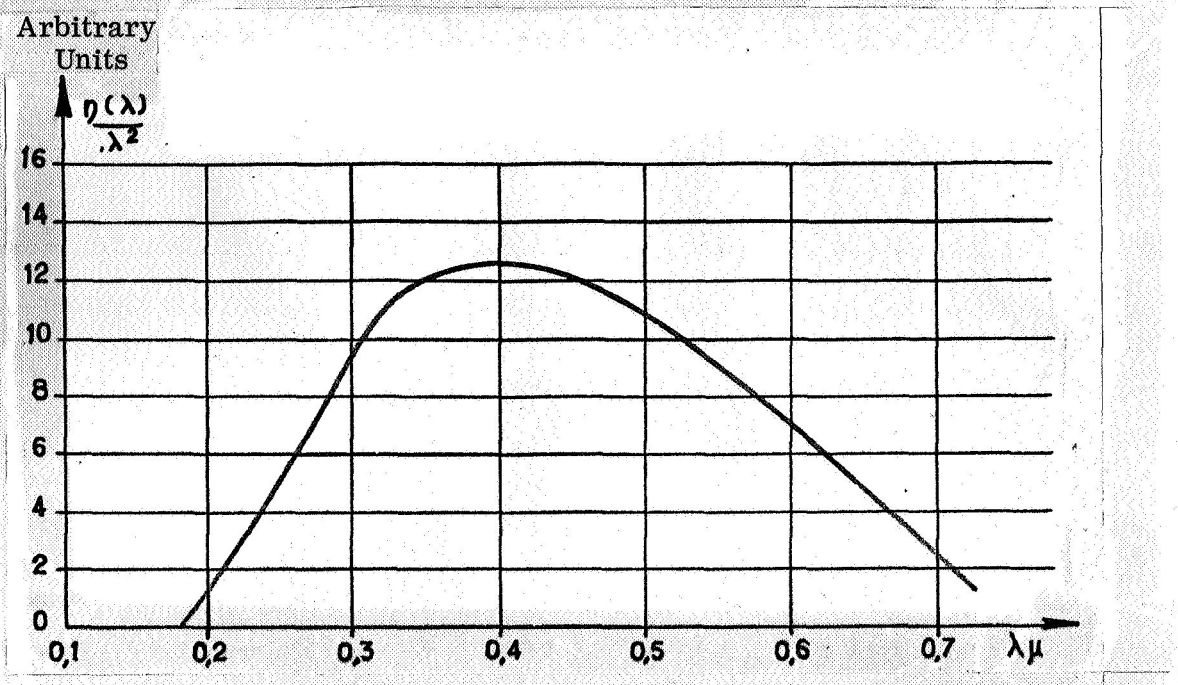

Figure 25. Spectrum of the Number of Photons.

II. ACTIVITY DETECTION /37

Having determined the performance of a beta detector using the Cerenkov effect, we shall study the causes which tend to limit its sensitivity and offer methods for improving it.

1. Characteristic Fluctuations and the Signal-to-Noise Ratio

The problem of signal detection is essentially one of reducing the background noise of the equipment. A detector is useful and sensitive only so long as the characteristic fluctuations – the number of pulses counted with no active sources present – is weak enough so that the presence of beta emitters will show up through a noticeable increase in the counting rate. If there are no characteristic fluctuations, the information capacity would be infinite since only the noise imposes an upper limit on it. A constant counting rate corresponds only to the characteristic fluctuations, and the "signal" is the variation of this counting rate. The background noise has three possible origins.

a. Thermionic Noise

Characteristic of photomultipliers is a "dark" current due to residual gas ionization, field emission at the tips, or primarily thermionic emission from the cathode and the first few dynodes. The intensity of this current varies according to Richardson's expression $AT^2 \exp(e\Phi/KT)$. One method for reducing this noise consists in reducing the temperature to -20° C; but then the equipment is difficult to handle and the sensitivity of the photocathode suffers.

Specially selected photomultipliers are therefore used. The tolerance allowed by the CEA and the Société radiotechnique (the Radio Engineering Society) for the 56 AVP-UVP series is a 511 A dark current for a gain of 10^8. For anode voltage pulses corresponding to a single electron only, there would be an output count of 300,000 cps which is much too large. The use of a photomultiplier with a dark current of less than 200 nA makes it possible to use the method of fast coincidence. This method permits counting pulses which arrive simultaneously over the two channels and eliminating single pulses. Since this can only be done during a finite time, the result is, as we shall see later, random parasitic pulses corresponding to the probability of two chance pulses occurring in this time.

Moreover, the signal is too weak (one or two electrons) to be picked out by simple discrimination from the background noise at a level which is at least its equal (thermal noise) if not higher (cosmic radiation).

b. Ambient Radiation

Since measurements are made by comparison with inactive water, its purity and the inactivity of the metal walls and the paint coating must be complete. In addition, a fixed radiation caused primarily by the walls and floor of the laboratory generates a quite considerable background noise. This involves gamma rays emitted by the K^{40} of the photomultiplier glass, the uranium and thorium of the materials surrounding the detector, as well as unstable gases in the atmosphere which are principally evident during the period of discharge of reactors (Argon 41) [17].

This radiation is reduced by a 5-cm thick lead housing. The cross section curves show that this would suffice to reduce the gamma flux of potassium 40 (1.45 MeV) to 10% of its value.

c. Cosmic Radiation /38*

This radiation at ground level is 80% of mu mesons and 20% of high-energy electrons. The total for this radiation furnishes about 1 to 1.5 particles per minute and per cm^2. Rossi and Asten assign a maximum of about 500 MeV to the spectrum of the mu mesons at ground level [18]. The Cerenkov threshold for the μ inwater is 50 MeV and the energy loss is of the order of 2.5 MeV/cm. Consequently, all the mesons traverse the vessel with a velocity of β close to unity.

The number of photoelectrons generated is then (see § I.5) for the vertical direction

$$N_{phe} = B \int_0^{10\,cm} \left(1 - \frac{1}{\beta^2 n^2}\right) dl$$

for high energies, and

$$N_{phe} = B \int_{E_{entrée}}^{E_{sortie}} \left(1 - \frac{1}{\beta^2 n^2}\right) \frac{dx}{dE}\, dE$$

for input energies E_e of about 50 MeV.

To trace the spectrum of mu mesons in the water, it is sufficient to know the meson flux per photoelectron for a given number of photoelectrons. The desired spectrum $\frac{dF}{dN_{phe}} = f(N_{phe})$ is derived from the spectrum given by Rossi in terms of the momentum, using the energy spectrum:

$$\frac{dF}{dN_{phe}} = \frac{dF}{dp} \cdot \frac{dp}{dE} \cdot \frac{dE}{dN_{phe}}.$$

A very sharp peak corresponds to the photoelectrons generated by the cosmic radiation passing through the entire volume.

This peak is very much attenuated if we take into account the spread of the fluctuations over the photomultiplier dynodes. If N_{phe} is the number of photoelectrons generated at the cathode, the average fluctuation σ is $1.2\sqrt{N_{phe}}$.

We must also bear in mind that all the mesons do not travel 10 cm, but have approximately such paths.

To continue the computations, we have chosen a reflector with a coefficient of about 0.85, which gives a B factor of 10 cm^{-1} with a UVP photocathode. We thus obtain 45 photoelectrons.

The cosmic flux per cm^2 per steradian and per second is $7.5.10^{-3}$ in the interval from 40 to 45 photoelectrons, and only $0.35 \cdot 10^{-3}$ between 35 and 30 photoelectrons.

The final spectrum is therefore very close to a statistical distribution centered at 45 photoelectrons. Other random phenomena such as luminous paths and amplifier background noise have a similar effect on the resolution.

To study directly the spread in pulse amplitudes due to cosmic radiation, we designed the equipment shown in Fig. 26. The pulses obtained at the anode of a photomultiplier are lengthened and amplified to permit the selector to study their amplitude spectrum under favorable conditions. A TPB-type plastic scintillator is placed under the tank. The mu mesons run through it in a path of about ten centimeters and furnish high-amplitude pulses which are used in coincidence with the pulses being observed.

The spectrum is shown in Fig. 29. There is a very large plateau, with a slight rise in the middle part, at the level of about 40 photoelectrons.

The cosmic radiation generates pulses larger than those of the signal itself. We can therefore eliminate the background noise due to cosmic radiation by means of an anticoincidence arrangement. An adjustable threshold permits discrimination, at the desired level, against the high-amplitude pulses to prevent their being counted.

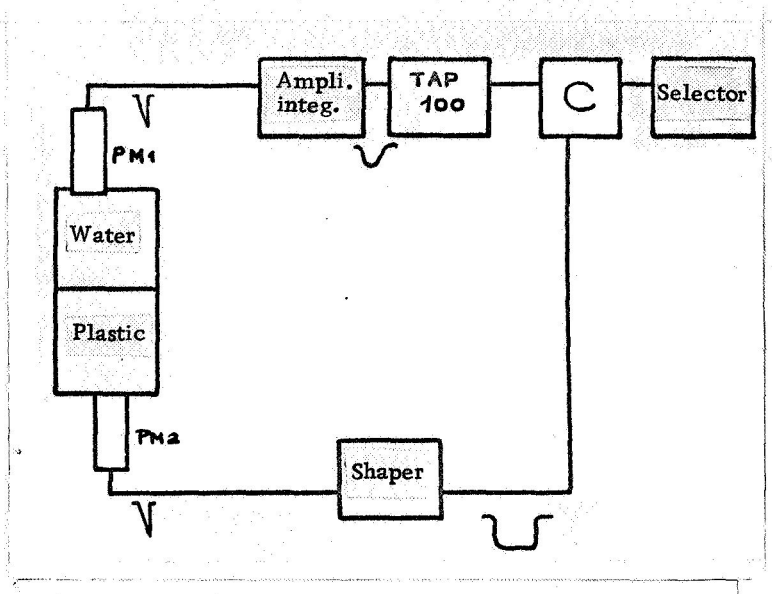

Figure 26. Equipment for Studying Cosmic-Ray Spectra.

2. Description of the Electronic Equipment

The block diagram of the equipment is shown in Fig. 30. The photocathode windows are in contact with the water. The pulses taken off the anodes are transmitted to the inputs of the coincidence circuit through two sets of stages, each containing a shaping preamplifier which calibrates the pulses by width and height, and a cable of variable length to allow for compensation of the difference in time of transmission between the two circuit paths.

An adjustable threshold at the output of the coincidence circuit permits elimination of the parasitic pulse which appears in only one of the paths. The anticoincidence signal is taken off one of the paths at a point where the amplification is still linear, before being amplified and stretched, so that the signal pulse arrives at the time the gate is closed. The counting is done by a counter circuit, type ECR2, with an input impedance of 100 ohms.

a. The Photomultipliers

Because the light level is very low and the phenomenon observed is fast, photomultipliers with high gain and low resolution time, of the 56AVP Dario type, must be used.

The optical characteristics of the input are designed to assure a good collection of photoelectrons. The voltages are set to establish a proportionate potential distribution among the neighboring dynodes providing the best signal-to-noise ratio [18].

The dynode bridge is made of 100 k Ω resistors to give a total output of 1.2 mA for 2000 supply volts. The potentials of the focusing anode and accelerator are adjustable by potentiometers. The stabilized power supply circuit is an ALS349, able to deliver 3.5 mA up to 3000 volts, positive, the photocathodes being grounded. The output impedance of the photomultipliers is 100 ohms, which permits observation on an

oscilloscope of the signal driving a device through a 100-ohm cable. The output pulse of the photomultipliers corresponds to very different emission levels.

If just one photoelectron is emitted, and if it gives an anode pulse of five nanoseconds at mid-height, the voltage across a 100-ohm resistor is

$$V = R\frac{Q}{t} = 0,3 \text{ v}$$

for a gain of 10^8.

Where there are some 40 photoelectrons, one must take into account the time constant of the light pulse. It is of the order of $3 \cdot 10^{-9}$ seconds if a very good reflector is used. The RC/θ factor is close to 0.6 for this particular equipment, and for a pulse height of the order of $0.3Q_0/C$ [20]. If N is the number of generated photoelectrons, G the photomultiplier gain, and e the charge of an electron, $Q_0 = NGe$. /42

We thus get a pulse of about 10 volts at the most. We note that the coefficient of reflection has a considerable effect on this height because of the total number of photoelectrons as well as the scintillation time constant.

b. The Preamplifiers

The preamplifier is mounted directly on the photomultiplier power supply, which obviates the need for a cable between the photomultiplier output and the preamplifier input. The preamplifier is designed to receive a pulse of 0.1 volt from the photomultiplier anode and shape it to drive the coincidence circuit for best results.

The tubes V_1, V_2, V_4, and V_5 are high-mu E188CC triodes (10 to 15 mA/V transconductance), and V_3 is a D3A pentode with a transconductance of 30 mA/V but with a plate resistance which is not negligible. The passband is improved either by high-frequency cathode decoupling or by an inductance in the plate circuit. /43

Thus, 15-volt output pulses are obtained for the coincidence input. The pulse-shaping is done by a short-circuited cable at the cathode of the penultimate tube (V_4). The propagation time for a 100-ohm cable of this type is of the order of five nanoseconds per meter. The time for the propagation and reflection is then 2.1×5.10^{-9} sec. The voltage pulse is reflected at the end, returns with an opposite sign, and is added with a delay of 10^{-8} seconds to the initial pulse.

The resultant pulse at the input to the 50-cm cable is shown in Figure 33.

Since this pulse-shaping is done during the signal rise time, the pulse height depends only slightly on the photomultiplier gain. We thus obtain pulses of the order of 4 volts at the coincidence circuit input. The residual pulse is grounded by a diode. The output impedance is low (100 ohms for the output and 100 ohms for the coincidence input) to avoid pulse-stretching.

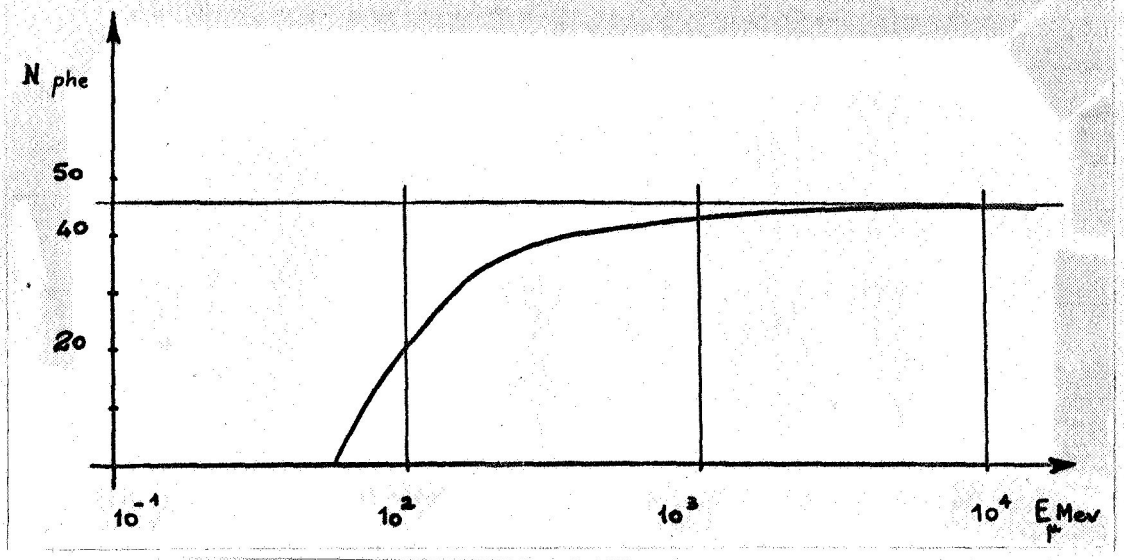

Figure 27. Number of Photoelectrons Per Mu Meson.

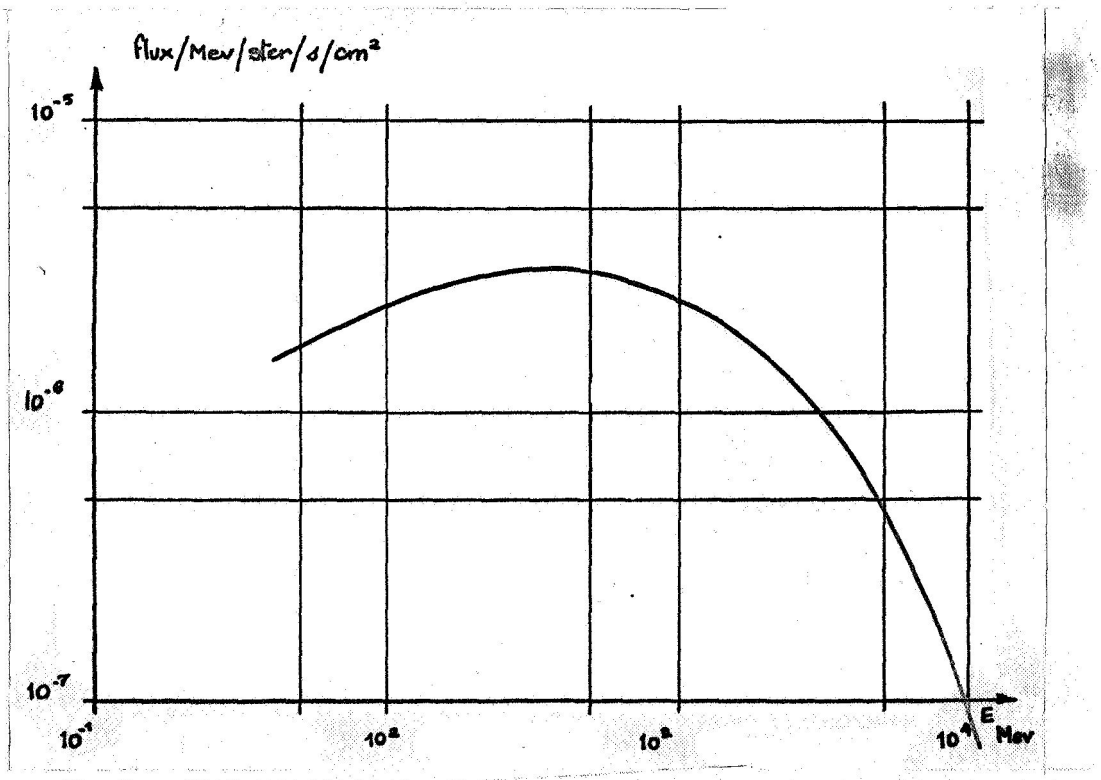

Figure 28. Energy Spectrum of Mu Mesons at Ground Level.

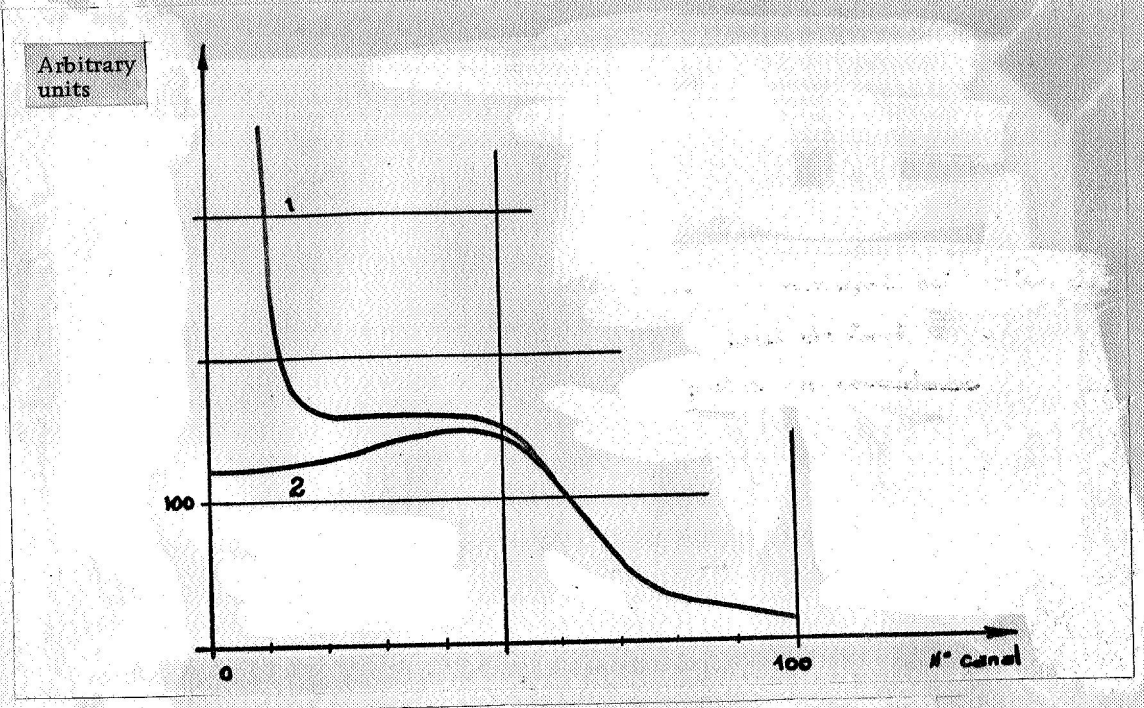

Figure 29. Spectrum Observed at the Selector.

1) Only one circuit path after elimination of the background noise;
2) Coincidence spectrum.

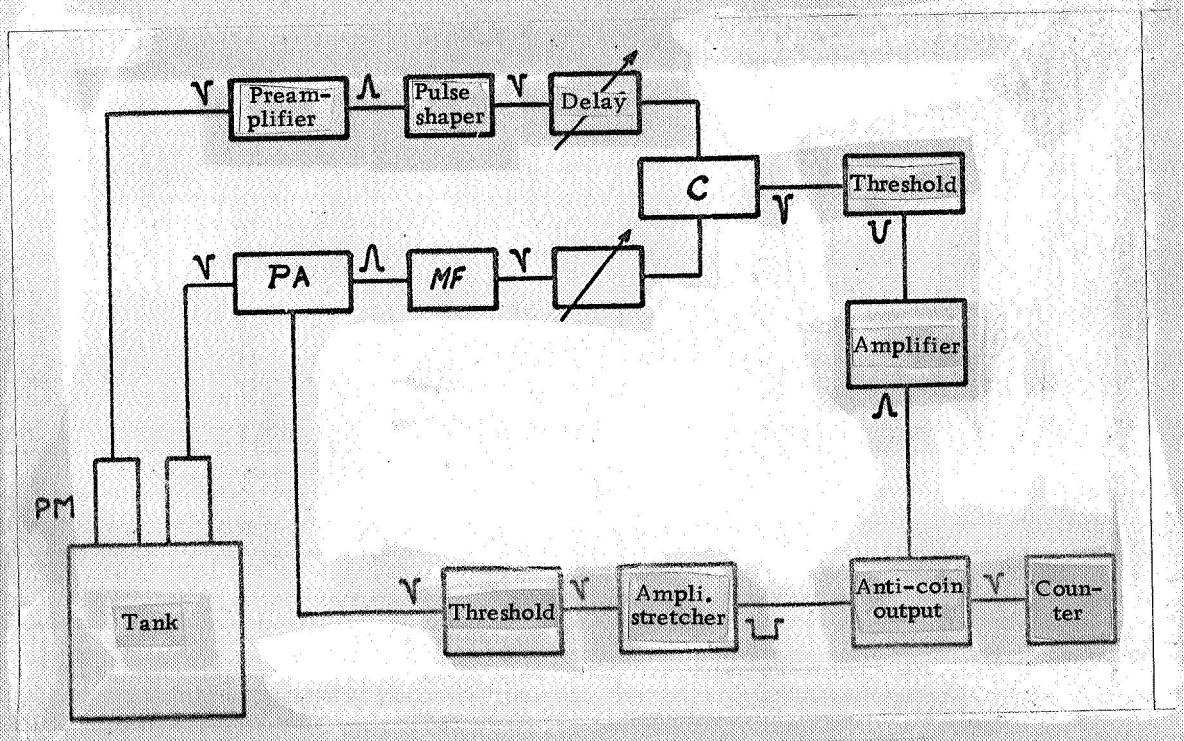

Figure 30. Block Diagram of the Detector.

/42

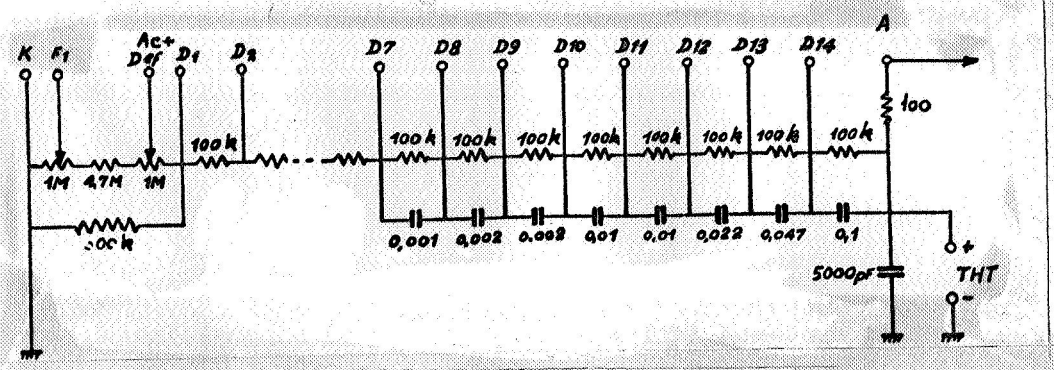

Figure 31. Photomultiplier Wiring.

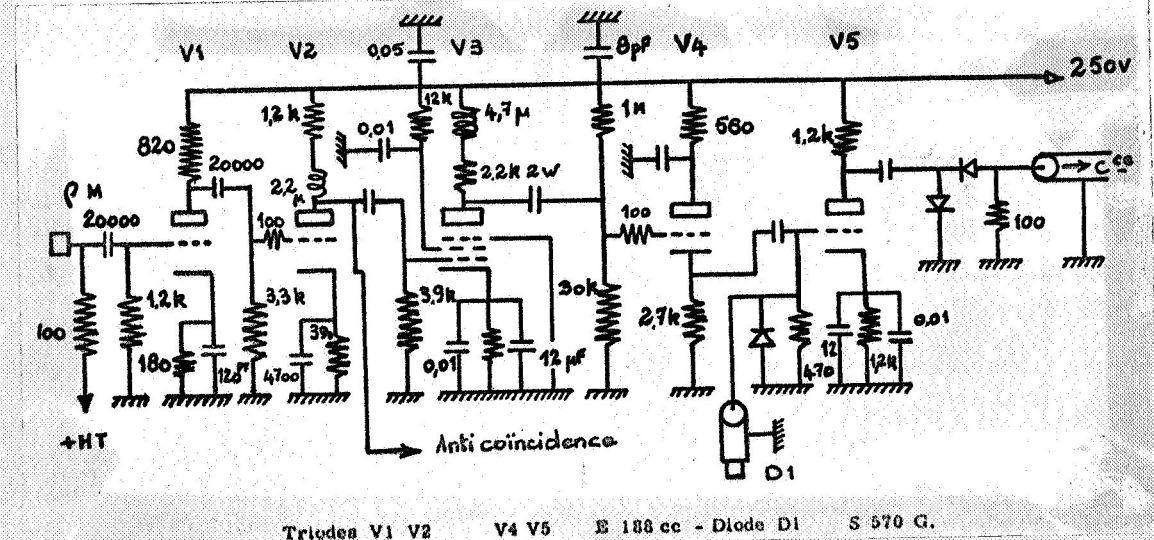

Triodes V1 V2 V4 V5 E 188 cc - Diode D1 S 570 C.

Figure 32. Pulse-Shaping Preamplifier.

/43

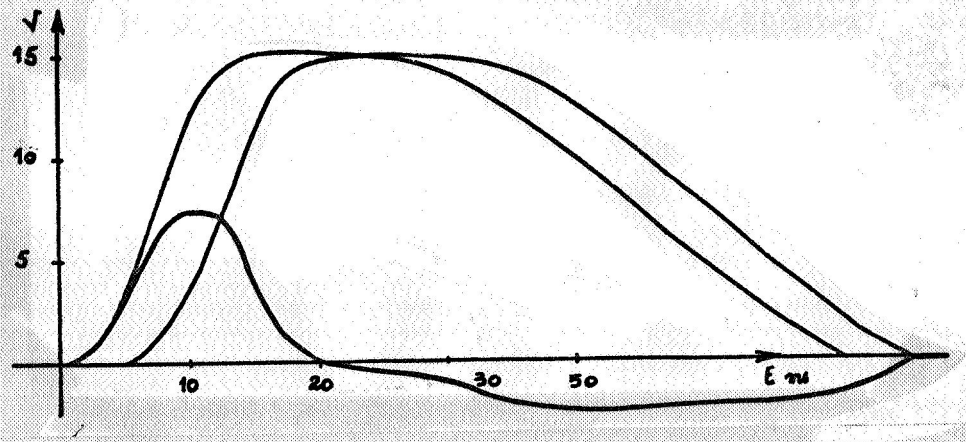

Figure 33. The Pulse after Shaping.

c. Coincidence Circuit

If a count of the coincidences between two photomultipliers were made, the rate would be $p_t = p_s + p_f$, where p_t is the overall rate, p_s is the rate of true coincidences, and p_f is the rate of chance coincidences. We note that if N is the number Cerenkov light pulses produced in time T and η is the detection yield of the system, the average number of coincidences for time T is

$$N_c = \eta N + 2\tau \frac{N_1 N_2}{T}$$

where τ is the duration of the pulse, if it is rectangular, or the half-width at half the height of the resolution curve [21], and $2\tau N_1 N_2/T$ is the number of chance coincidences. Thus, the effect of the chance coincidences increases

a) with the noise N_1 and N_2, which imposes the choice of the selected photomultipliers;

b) with the resolution time τ, which impels us to use a rapid-coincidence circuit. /44

Also, the relative effect of the background noise decreases as the time of measurement T increases. We shall discuss the choice of this measurement time at a later point (§ II, 4a).

By using cables of various lengths for the delay of one circuit path with respect to the other, we can measure the coincidence count (Figure 34).

We obtain a curve which has steep sides only when the pulses are rectangular. The delays are adjusted to the curve maximum. It can then be shown [22] that the resolution time

$$\tau = \frac{1}{2 N_{max}} \int_{-\infty}^{+\infty} N(t)\, dt$$

is really the half-width at half the height. Evidently, for a very large delay, the counting rate reduces to chance coincidences;

$$n_f = 2\tau n_1 n_2$$

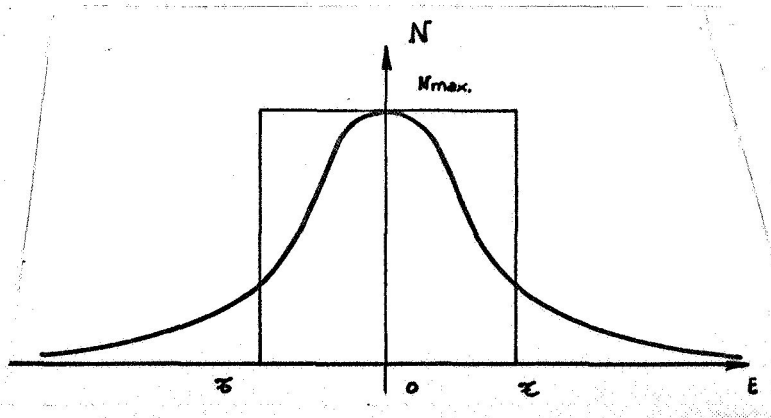

Figure 34. Resolution Curve of a Coincidence Circuit.

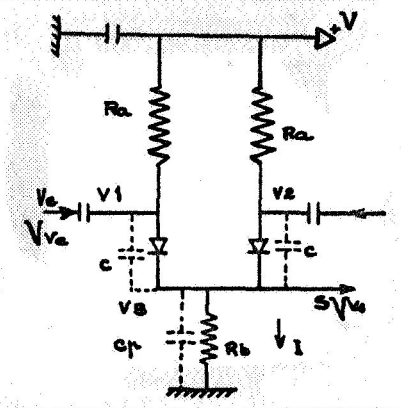

Figure 35. Basic Coincidence Circuit.

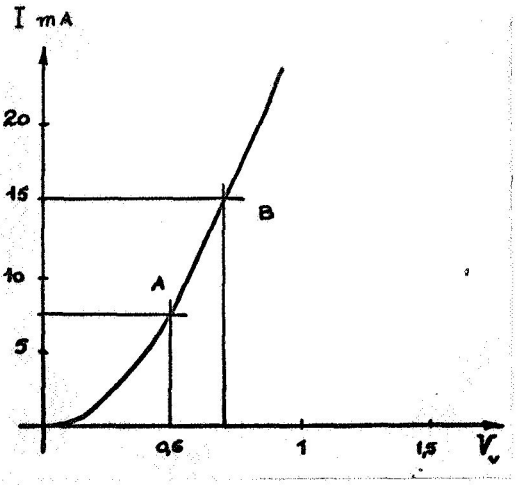

Figure 36. Diode Characteristic.

The circuit used is a diode AND circuit [22]. The input is a 100 ohm resistance into which negative pulses are fed. The operation is as follows. The pulses have a duration of a few nanoseconds; consequently, the time constant of the circuit must be at a maximum of the same order. For this reason, we use a relatively low resistance for R_b, thus:

R_b = 560 ohms (see Figure 35); C_p = 10 pf.

Operation:

1) In continuous operation, the current I is distributed equally between the two diodes, and the operating point on the characteristic is at A (Figure 36).

2) At the arrival of a single pulse, the corresponding diode blocks. Since the total resistance of the circuit varies from $R_b + R_a/2$ to $R_b + R_a$, i.e., on the order of 10%, the supply current I is practically constant and is carried over to the other diode. The operating point then switches to B. When this occurs, a signal appears at what is known as the rejection output. This signal consists of

a) part of the amplitude proportional to the input CV_e/C_p, but decreasing with a low time constant (less than 10^{-9} seconds for C ~ 1 to 2 pf with an S570G diode);

b) a so-called "rejection" corresponding to the transfer of the operating point on the characteristic from A to B. /45

We thus have the respective equations: a) in static operation: $V_3 = V - (Ra\ 1/2 + Rd\ 1/2)$ where Rd's the forward resistance of the diode.

b) with a pulse, $V'_3 = V_3 - (R_a I + R_d I)$, or $V'_3 - V_3 = (R_a + R_d)\frac{I}{2} = V_r$.

We can thus see that this parasitic pulse is not a function of the input signal. To obtain better sensitivity for the signal, V_r must be reduced, and consequently the current I. With R_b present, V can be reduced. However, a compromise occurs, for V has an equal effect on the maximum output amplitude in coincidence.

3) With an input of two simultaneous pulses, the diodes block for $V_e > IR_d/2$ and /46 the voltage tends to zero until the point where the voltage $V_3 - V_1$ or $V_3 - V_2$ (the lowest

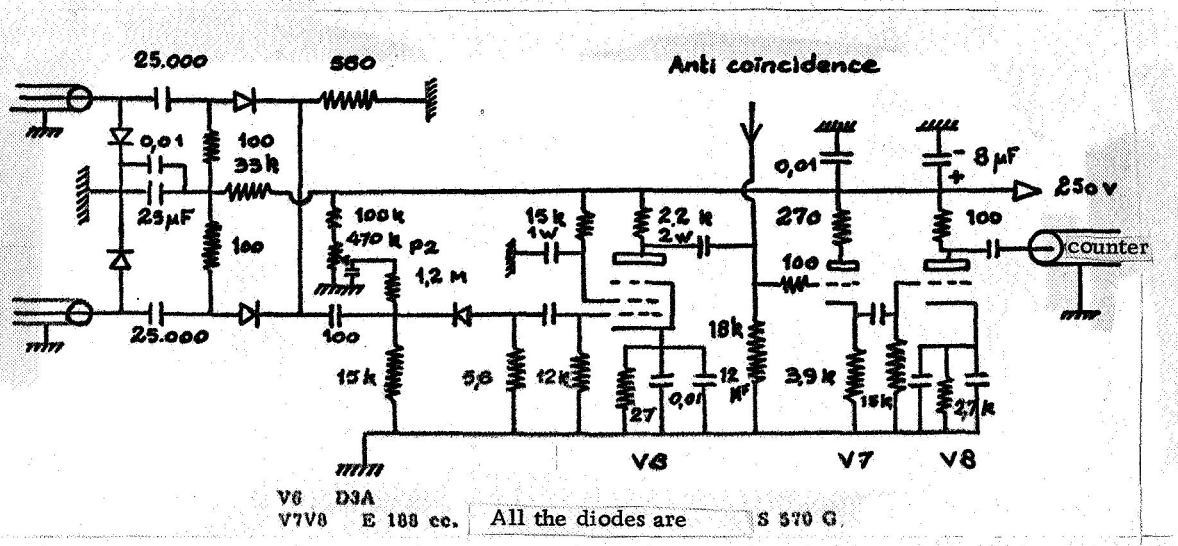

Figure 37. Coincidence Circuits and Input to the Counter.

of the two) becomes negative. At this point, the corresponding diode conducts. Then, a pulse appears at the output with a height equal at most to the input voltage, which is $V_e - IR_d/2$, and which rises with the time constant θ.

The ratio V_s/V_r, of the order of 10, is the sensitivity of the circuit.

Parasitic pulses are eliminated by a variable threshold, allowing only the strongest pulses in coincidence to pass. However, the distributed capacitance of the diode permits the passage of a parasitic signal of 0.5 volts after amplification. In that case, it is sufficient to adjust the counter to one volt. The coincidence pulse is brought to a level of 7 volts across 100 ohms for a duration of 80 ns to drive the counter under optimum conditions.

d. The Anti-Coincidence Circuit

We have seen, in § II.1c, that cosmic radiation gives rise to strong pulses. An adjustable threshold allows amplifying only those pulses before stretching them, thus transmitting them in anti-coincidence (Figure 38). The threshold diode must transmit the signal quickly and allow the passage, through its capacitance, of only a small part. This small portion is eliminated by a second polarized diode encountered before the second amplification.

We thus obtain a negative pulse of 40 volts which blocks tube V7 until the positive signal coming from V6 appears. Thus anti-coincidence occurs.

3. Detector Operation

Numerous parameters, such as the reflector used, the high voltage applied to the photomultipliers, the input threshold for the counter, the coincidence time, the types of photomultipliers used, are involved in the detector circuit operation.

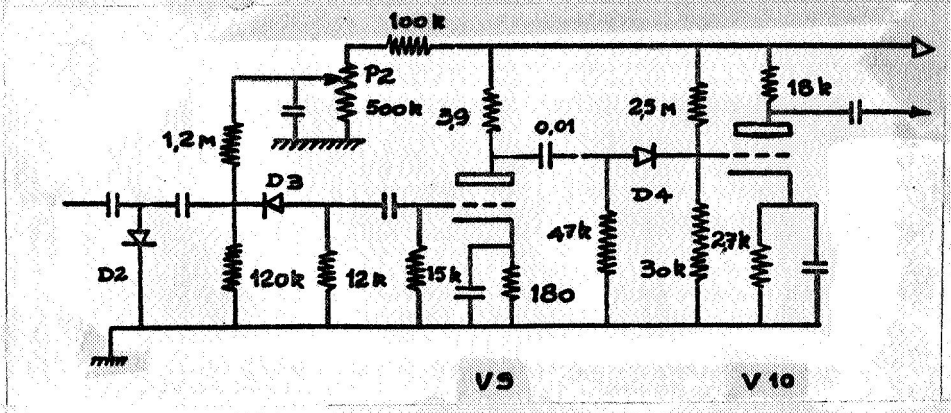

Figure 38. Anticoincidence Circuit.

V9 and V10	E 188 cc
D3 and D 4	OA9
D2	S570 G.

For our first series of tests, we chose 56UVP photomultipliers selected for their low background noise, and a reflecting material of white paint baked in a kiln.

a. Pulse Spectrum at a Photomultiplier Output

The curves of Figure 39 show the pulse spectrum yielded by a photomultiplier.

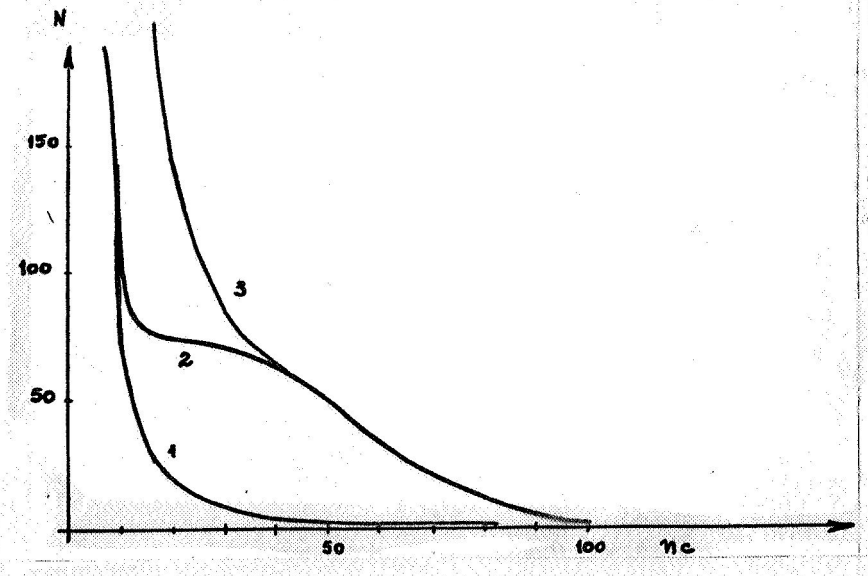

Figure 39. Pulse Spectrum at the Photomultiplier Output.
1) Background noise; 2) Total noise with water; 3) Spectrum with $5 \cdot 10^{-6}$ μc/cc of S_r90

The photomultiplier background noise, for a temperature of 23° C, is large only in the initial channels. The characteristic fluctuation of the detector (thermal noise, ambient gamma radiation without the lead housing, cosmic radiation) produces the plateau we have already seen in § II. 1c.

The spectrum due to the additional activity from the Sr^{90}-Y^{90} source of $5 \cdot 10^{-6}$ μc/cc shows that the emitter action makes itself felt below the 40th channel, i.e., at the cosmic radiation level. We can only conclude that this corresponds to the maximum number of photons seen by the photocathode rather than the maximum energy of the beta spectrum. Indeed, for $5 \cdot 10^{-6}$ μc/cc, or 11,000 dpm/liter, we should get 100,000 impacts in 30 minutes on one photomultiplier. But this high counting rate, corresponding to an emission of from one to two photoelectrons, occurs in the first 10 channels. As for the portion of the spectrum between the 30th and 40th channel, where the signal counting rate is of the order of 50 per channel in 30 minutes, this is due to the disintegrations near the photocathode which are collected, under optimum conditions, with an optical yield close to unity. Under these conditions, some 50 photoelectrons can be obtained.

b. Adjustments and the Choice of Operating Point

1) Since the photomultipliers are 56UVP's which operate at 2300 volts, we have recorded the curve for the counting rate of the characteristic fluctuations outside the lead housing, in coincidence, and adjusted the focusing voltage to the maximum of the counting rate. This voltage is in the neighborhood of 12 volts.

2) We have recorded the curve for the count rate of the total noise in coincidence as a function of the counter threshold, with and without the lead housing. The housing reduces the background noise by a factor of two regardless of the threshold chosen. With a lead housing 5 cm thick attenuating the ambient gamma flux by 90%, one can observe some 30 counts per minute due to the remaining 10%. (Figure 40).

3) Absolute counting rate at the coincidence input. The curves correspond practically to the thermal noise of the B7850UVP and B7853UVP photomultipliers. We can see that there is an appreciable difference in the background noise between these photomultipliers for a given high voltage. For a noise rate of 50,000 cpm, there is a 300-volt difference between each of the applied high voltages (Figures 41 and 42).

4) The curve for the total signal-to-noise ratio in coincidence shows no maximum in the zone of interest.

We recorded the noise rate in coincidence, as a function of the high voltage applied /48
to the photomultipliers, as well as the signal counting rate furnished by a supplementary activity of $5 \cdot 10^{-7}$ μc/cc from Sr^{90}-Y^{90}. The two curves evidently increase, but their ratio increases equally with the applied high voltage. As the number of chance coincidences increases, the gamma yield improves. This precludes the existence of an optimum point. However, we can choose a zone of operation between 2000 and 2400 volts, depending on the kind of reflector used. There is a risk that the stability will suffer if the voltage is higher.

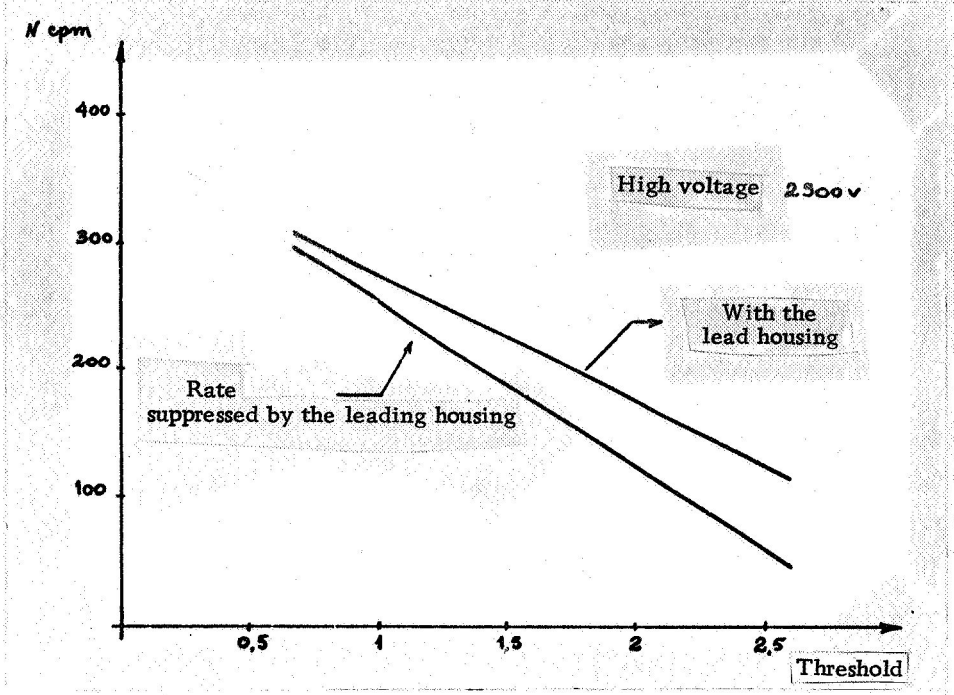

Figure 40. Action of the Lead Housing.

c. Coincidence Resolution

The resolution curve (Figure 43) of the coincidence system shows the output counting rate as a function of the delay in one signal path compared to the other. This delay is measured by the difference in length of the cables between the preamplifiers and the two coincidence circuit inputs, at the rate of 5 nsec per meter. To obtain a sufficient counting rate, we use a source of 5.10^{-6} μc/cc of Sr^{90}.

The time in which the gate is open corresponds to the half-width at mid-height of this resolution curve. We have established, moreover, that all these curves have a maximum for a delay corresponding to 25 cm of cable.

Finally, we use a high voltage of 2300 volts as the operating point, except with a threshold of one volt on the counter.

d. Study of Chance Coincidences

For the point defined above, the counting rates at the input to the coincidence circuit are 26,000 cpm and 1,800,000 cpm, respectively. The rate of chance coincidences should be $2\tau N_1 N_2$ if τ is the time during which the gate is open, as determined by the resolution curve. This time is 12.5 nsec, which gives 20 cpm for a one-volt threshold.

1) We have studied the rate of chance coincidences as a function of the high voltage for the photomultipliers. The voltage applied to the B7850 is the abscissa in Figure 45,

and the difference v applied to the B7853 photomultiplier, where $v = V_{3U} - V_{0U}$, is the parameter. The counting is equally cognizant of the clickings which can be produced in one photomultiplier and the effects seen after reflection from the bottom by the other photomultiplier. Only the chance coincidence effects are obtained; this is done by covering the quartz windows with an opaque screen. We have studied these effects for a voltage of 2300 volts as a function of the threshold: the clickings can be estimated at /56
3 cpm on the average (Figure 46).

2) It is also worthwhile to study the effect of the temperature on the counting rate for each circuit path and, more precisely, on the rate of chance coincidences. Between 15 and 40° C, the rate is multiplied by a factor of 10. Around 23° C, a variation of 1.5 cpm per degree C is recorded (Figure 47). The variation is $\Delta Nf = 2\tau [N_2 \Delta N_1 + N_1 \Delta N_2]$, bearing in mind that τ is not varied.

If we make the reasonable assumption that $\Delta N_2 = \Delta N_1 \frac{N_2}{N_1}$, we then get $\Delta Nf = 4\tau N_2 \Delta N_1$, which leads to a variation of 10^3 cpm for N_1 in the absolute counting rate per degree C, and of $70 \cdot 10^3$ cpm for N_2. This variation of 1.5 cpm per degree is in the domain of the statistical variation for a counting time of 10 minutes.

$$\sigma_{10} = \frac{\sqrt{10\ N_{cpm}}}{10} = 1,4 \text{ cpm.}$$

e. Volume Homogeneity of the Source

We performed an experiment with a solid source of strontium-yttrium 90, type SB_1. This, almost a point source, has a plexiglass support 50 mm in diameter and 6 mm thick. The radioactive solution, covered by varnish, is at its center. The assembly is protected by a very thin plexiglass window (Figures 48 and 49).

We raised the coincidence counting rate as a function of the distance between the source and the plane of the photocathodes. For 0.1 μc, which is 222,000 cpm, we can expect a yield in the neighborhood of 10%, or 20,000 cpm. For distances varying from 2 cm to 10 cm, the counting rate does not vary 25%. We can therefore say that the detection yield is uniform.

f. Use of Converters

A series of experiments were made with 56AVP photomultipliers using dissolved light frequency converters. These devices have the property of transforming part of the ultraviolet spectrum into the visible range, thus permitting the use of photomultipliers without a quartz window. Two types of organic converters were tried.

We observed an increase of the order of 100% in the signal counting rate. Unfor- /57
tunately, it was accompanied by an increase in background noise.

Of the two converter substances used, 2-naphthylamine disulfonic acid in a concentration of 15 mg per liter of water [24] seems more effective as far as the counting rate

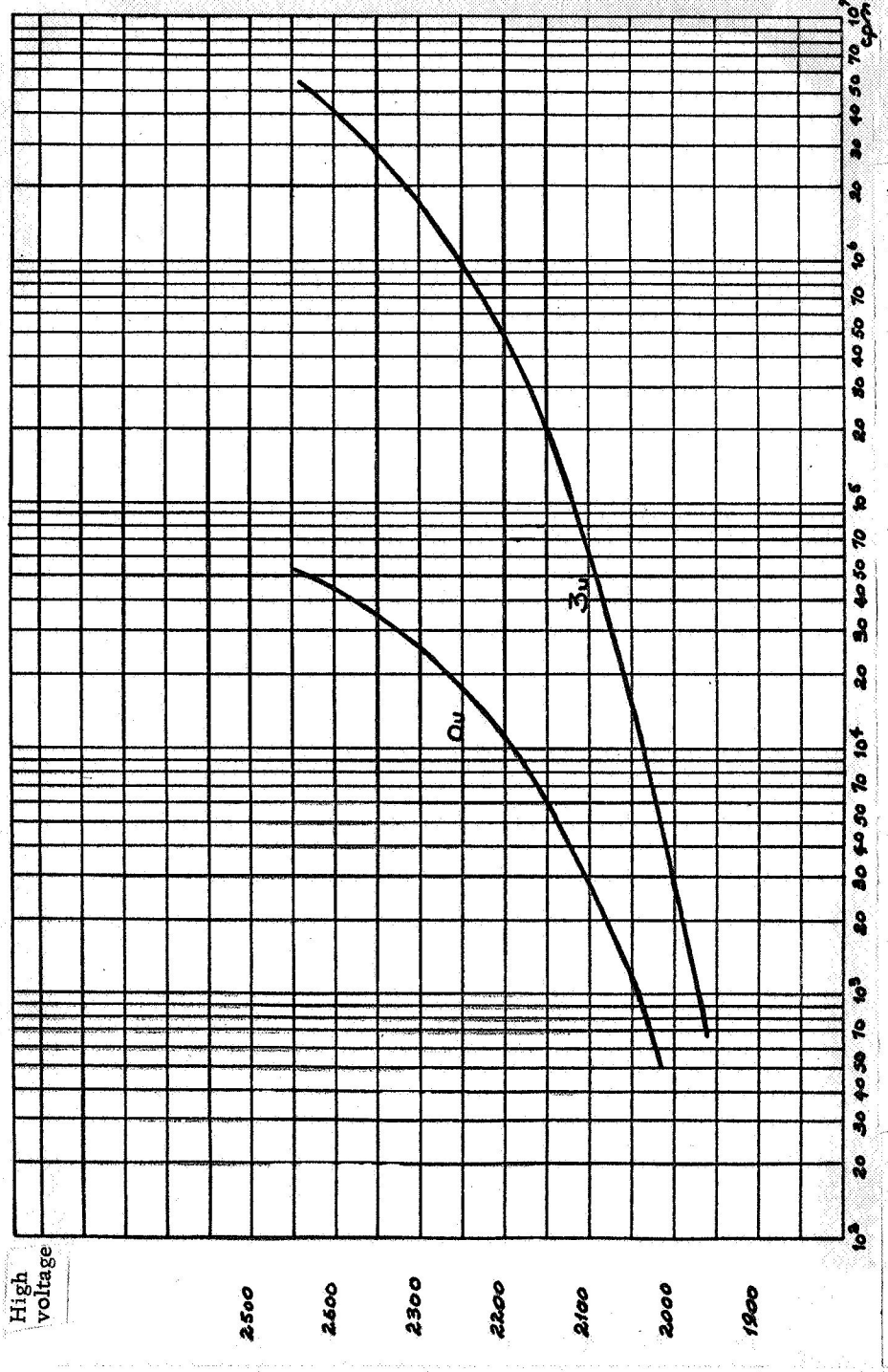

Figure 41. Preamplifier Counting Output (50 ohms, 1 V Threshold).

/50

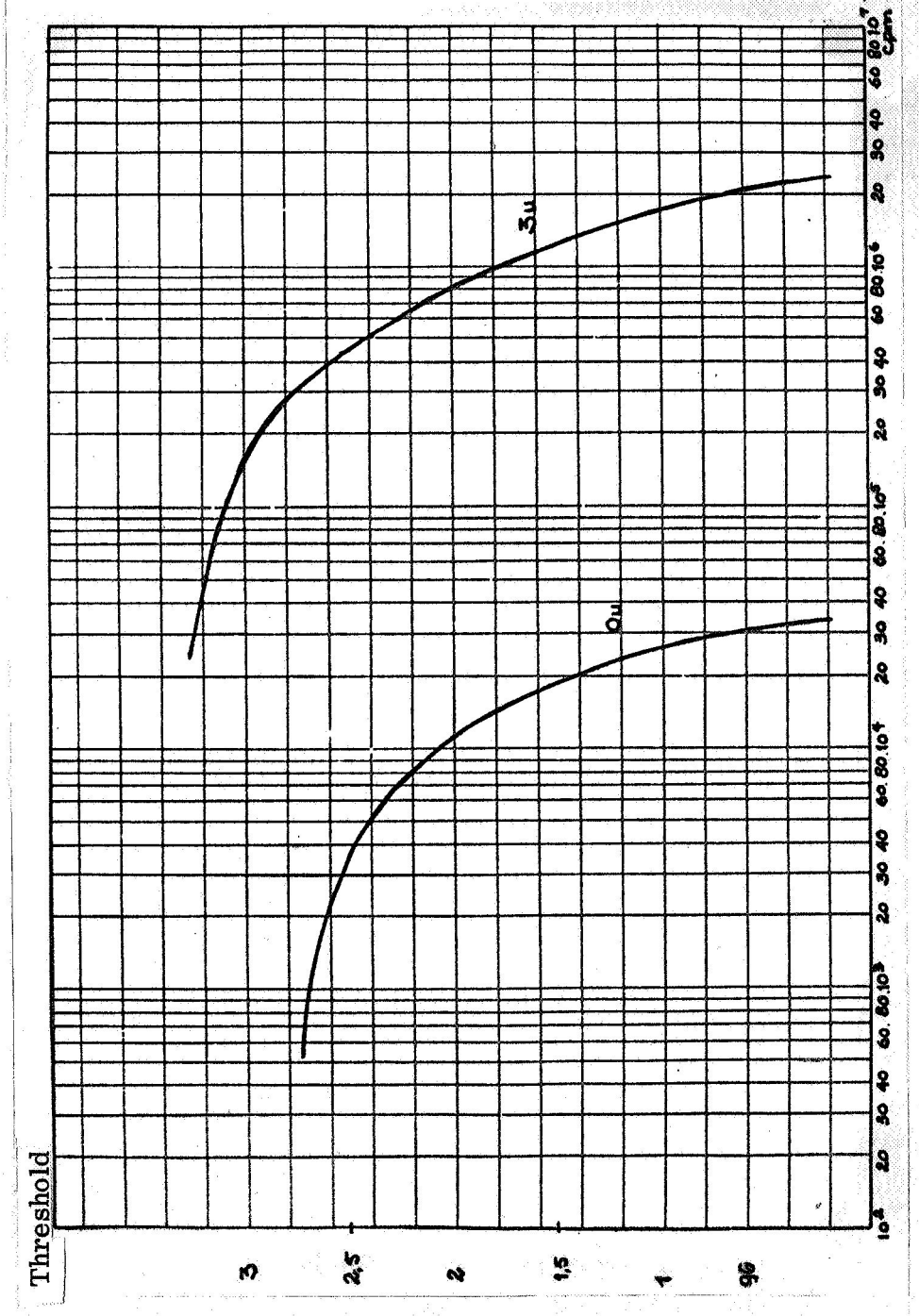

Figure 42. Total Count, at 2300 V High-Voltage.

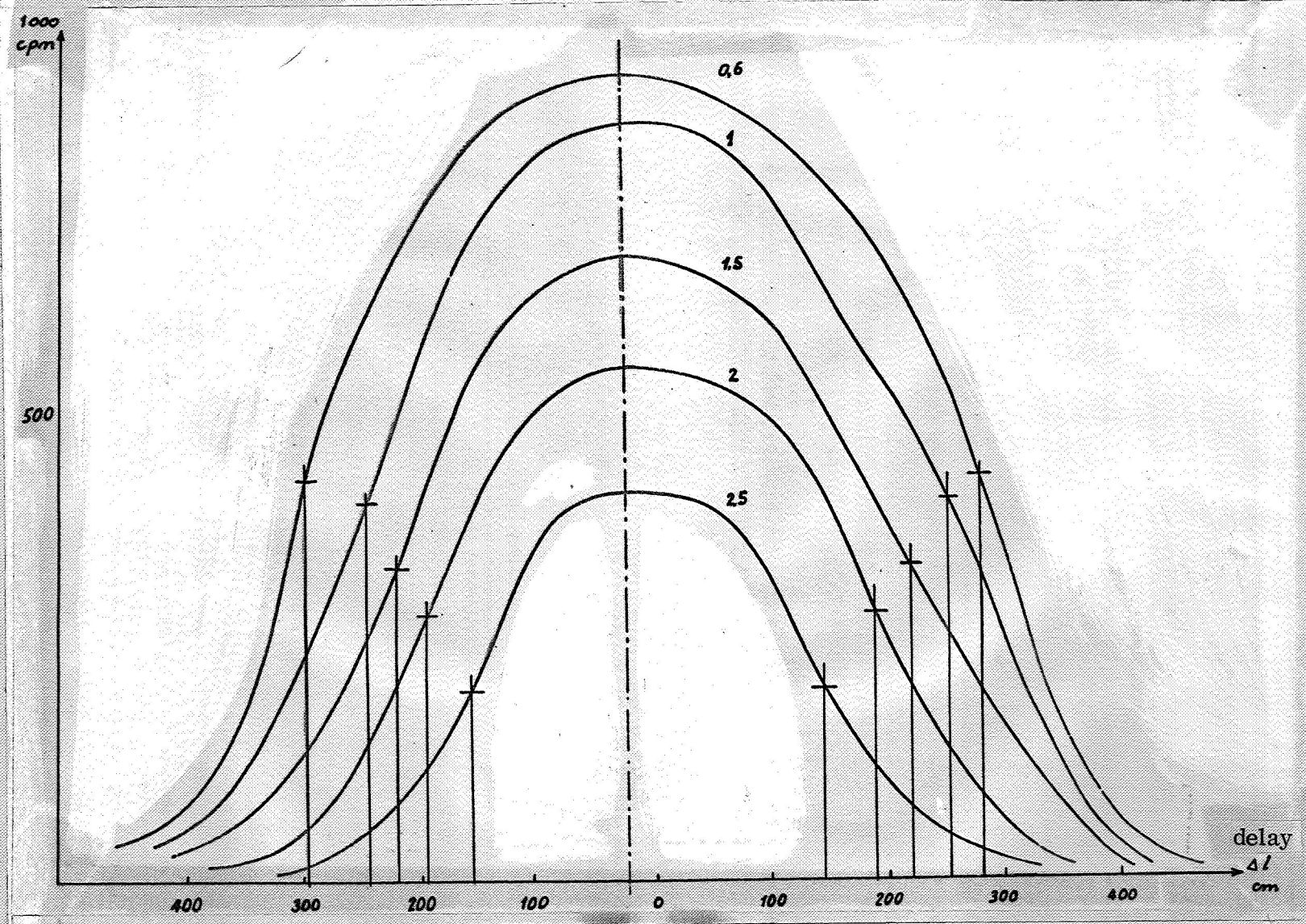

Figure 43. Resolution Curves; the Parameter is the Counter Threshold with a High Voltage of 2300 V.

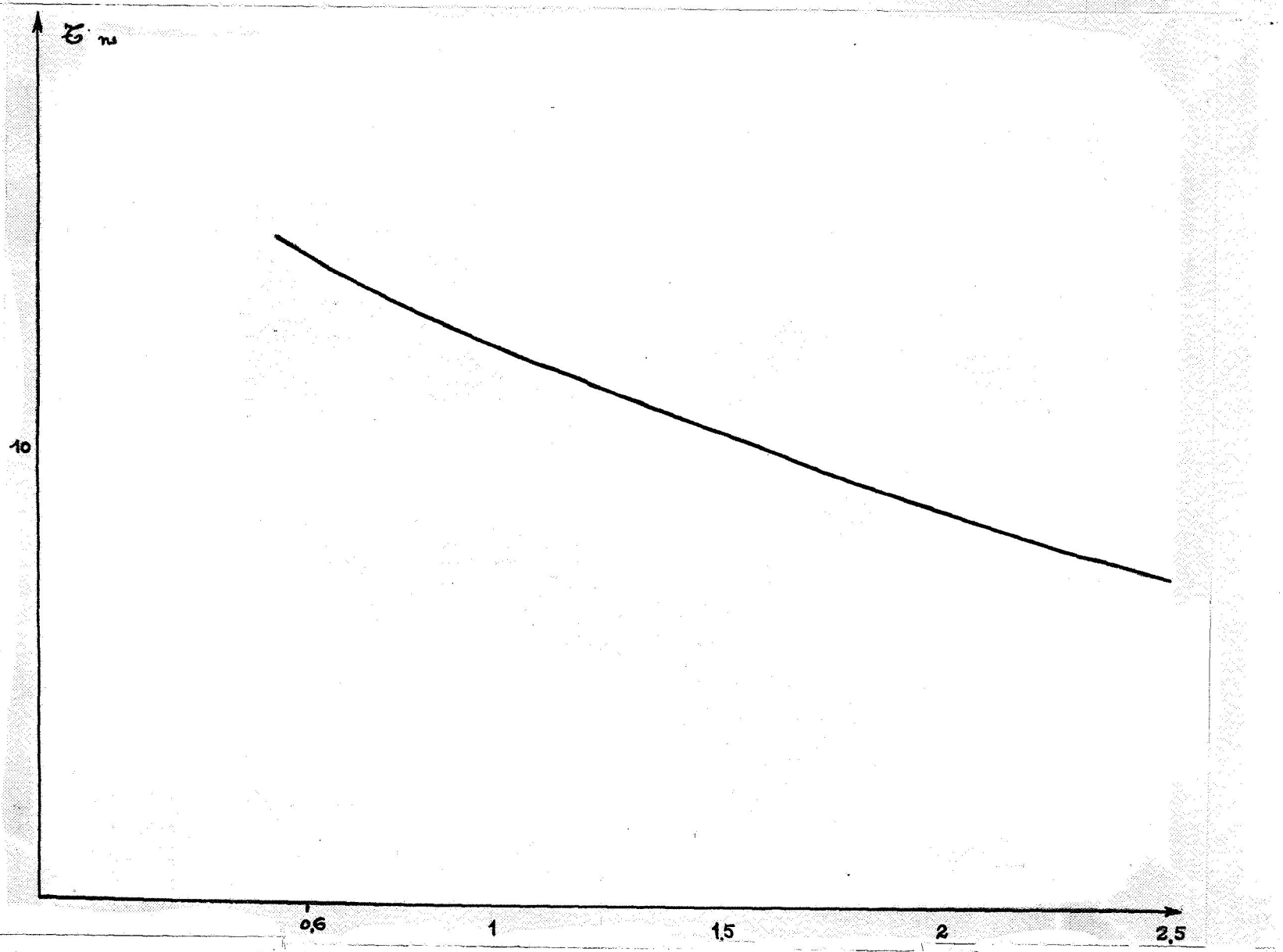

Figure 44. Gating Time as a Function of the Threshold.

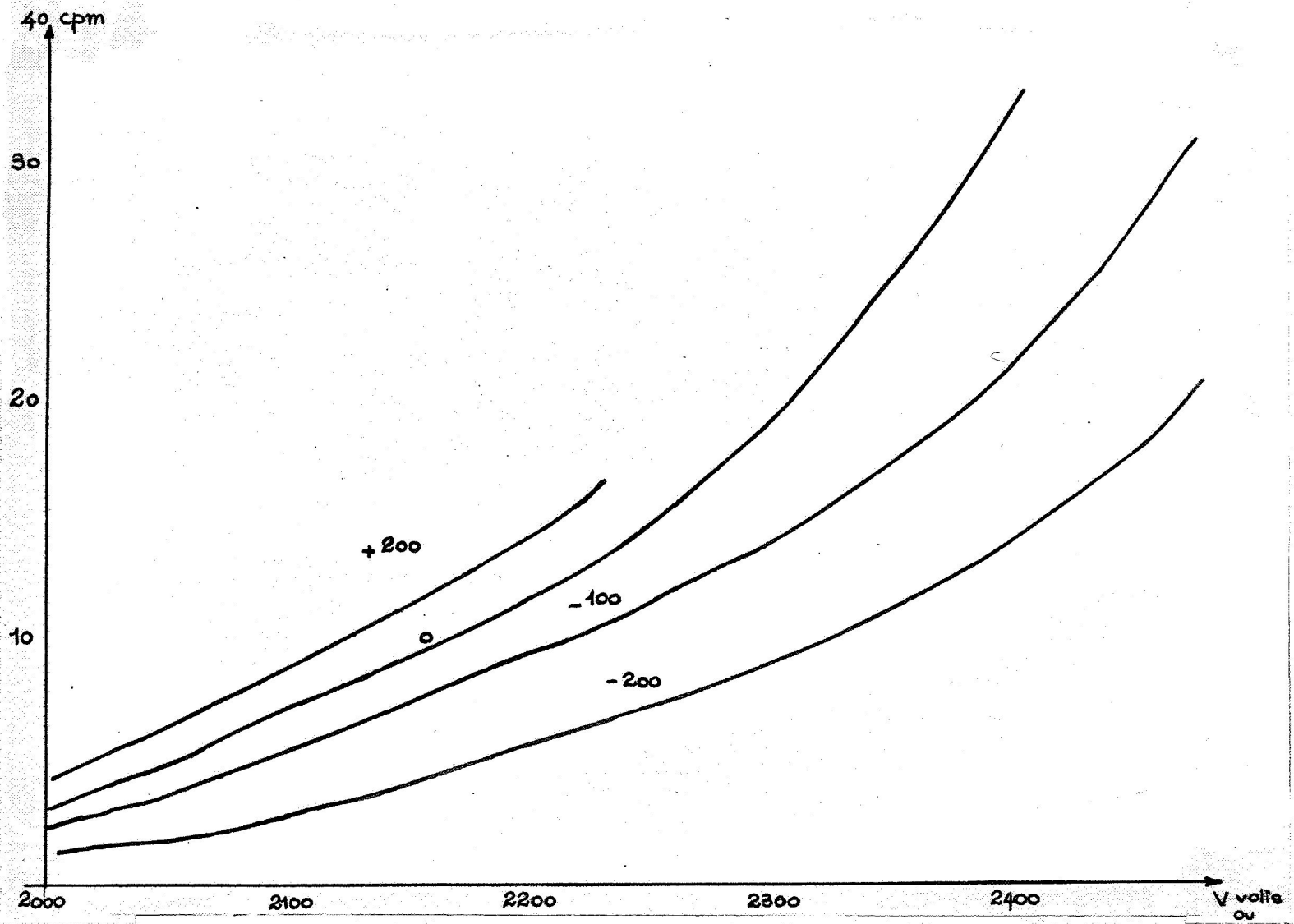

Figure 45. Chance Coincidences as a Function of Applied High Voltage; $V_{3U} = V_{0U} + v$.

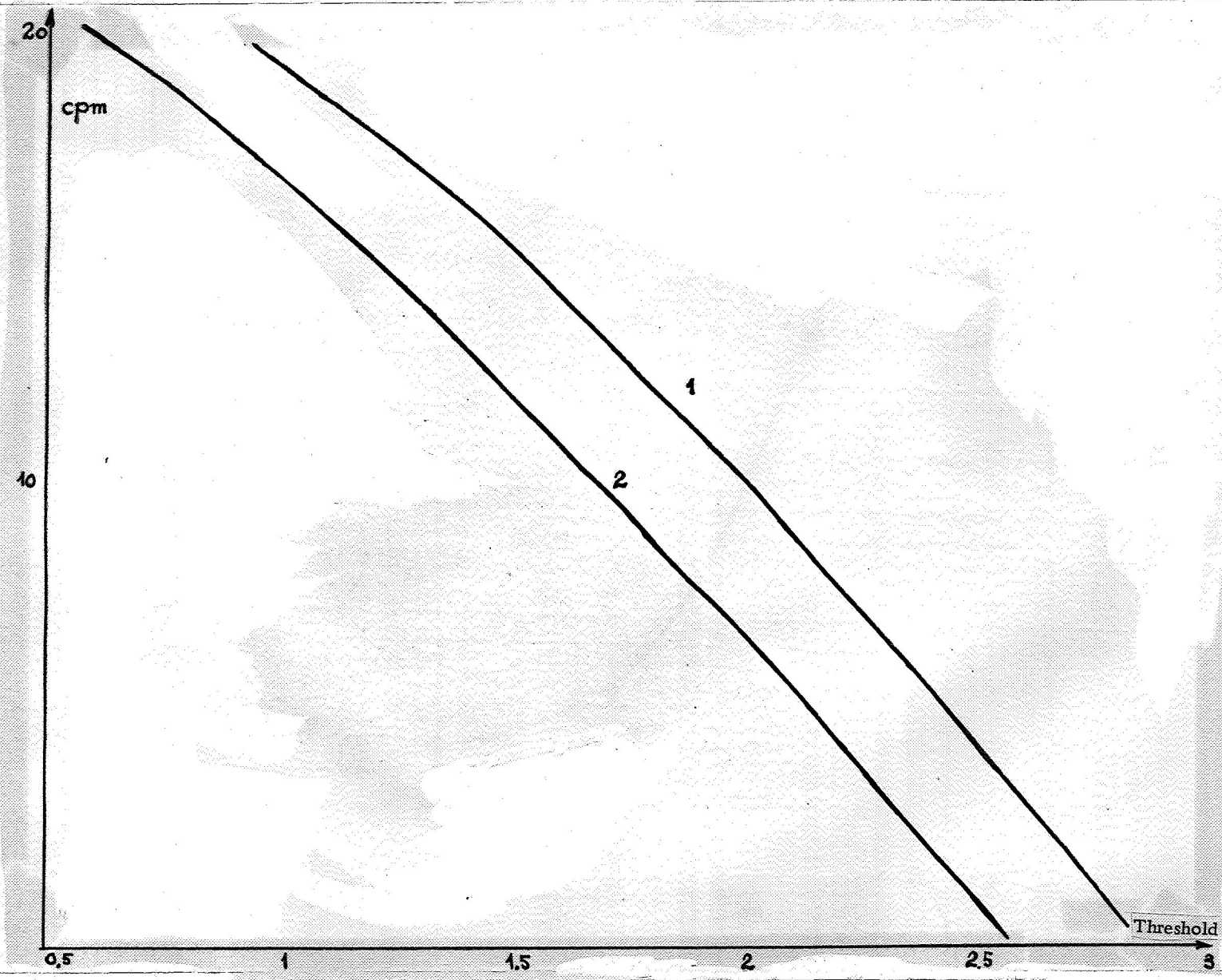

Figure 46. Two Chance Coincidences, One Chance Plus Clicking.

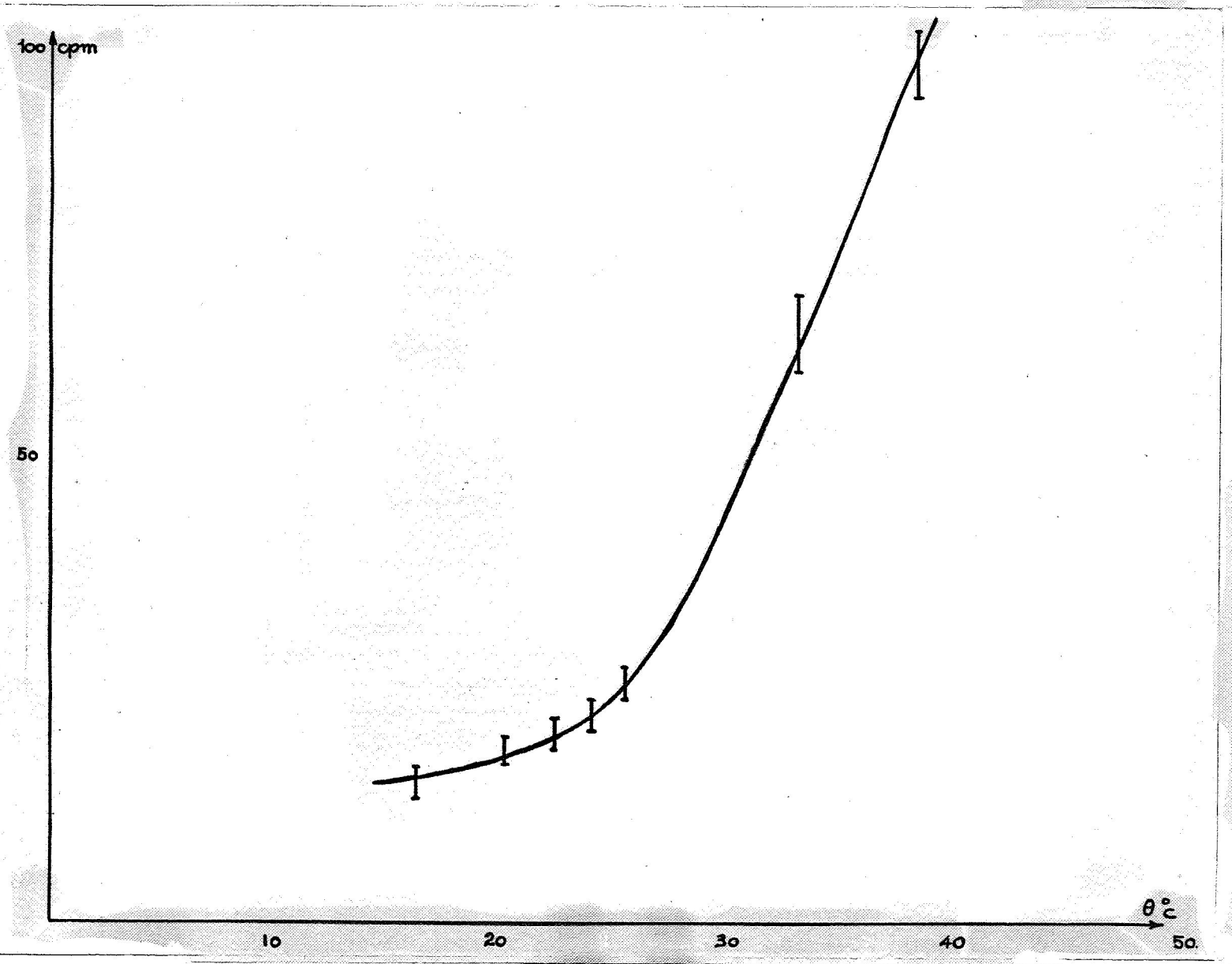

Figure 47. Rate of Chance Coincidences as a Function of Temperature.

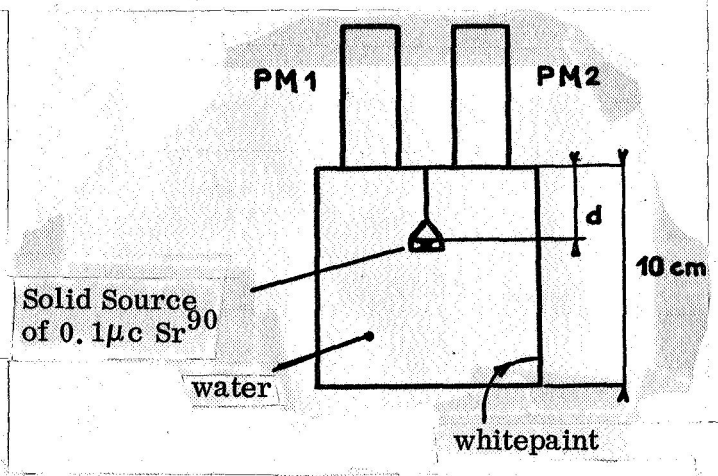

Figure 48. Equipment for Studying Detection Homogeneity.

is concerned than the β - methyl-umbelliferone in a concentration of 0.05 g/liter [25]. However, the highest improvement in the signal-to-noise ratio (50%) is not sufficient to recommend such converters, which have the additional drawback of making the measurement more sensitive to disturbance.

4. Detecting Contamination by Sr^{90}

a. Sensitivity and Time of Measurement

Our purpose is to detect activity equal to a tenth of the permissible dosage; i.e., 8.10^{-8} μc/cc in drinking water, which corresponds to 180 disintegrations per minute per liter. The detector yield should be such as to lead to an appreciable increase in the counting rate due to the characteristic fluctuations alone. The experiment was performed in two equal time durations T. At first, pure water is introduced into the vessel and we count the characteristic fluctuation N_b. Then the water to be tested is compared to it, giving a count of N_t. Since the two measurement times are equal, the net activity is

$$a = n_t - n_b = \frac{N_t - N_b}{T}$$

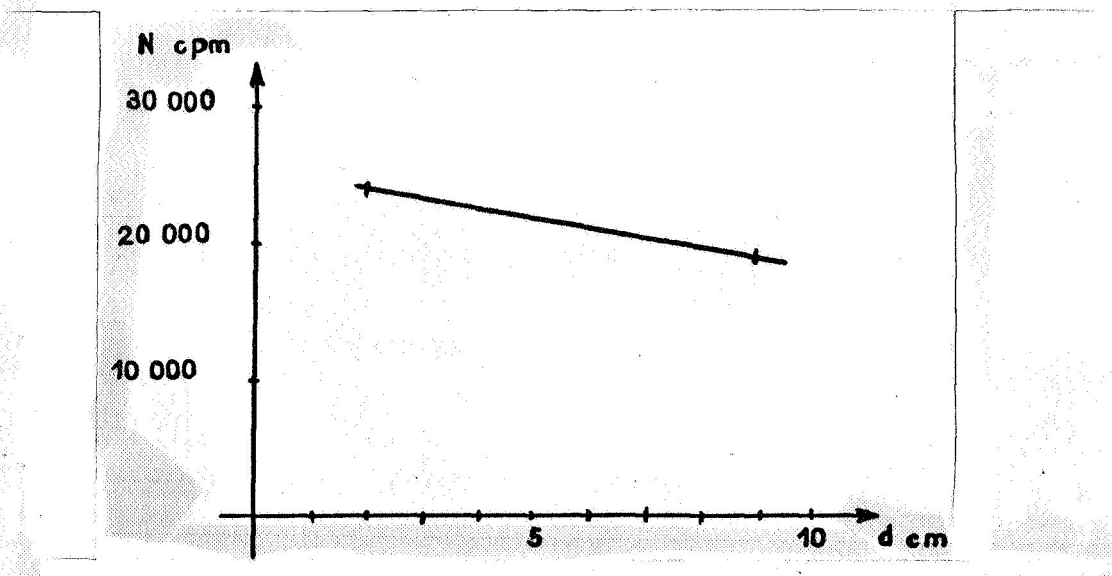

Figure 49. Counting as a Function of Distance from the Source.

If m_b and m_t are the true counting rates, and if the distribution of the experimental values is normal around the average value, the probability that one such value, n_b or n_t, is away by more than u_b and u_t from the average value is

for		
	$u = \sigma$ mean square difference	68.3%
	$u = 2\sigma$	95%
	$u = 2,576\sigma$	99%.

The best possible estimate of the activity is

$$m_t - m_b \simeq (n_t \pm u_t) - (n_b \pm u_b)$$
$$= n_t - n_b \pm \sqrt{u_t^2 + u_b^2} .$$

It can be shown [16] that $n_t - n_b$ is normally distributed around the exact mean rate with a mean square error of $u_{t-b} = \sqrt{u_t^2 + u_b^2}$. An activity would be detectable with a reliability of 99% for a counting rate higher than $\sqrt{u_t^2 + u_b^2}$ or $2,576\sqrt{\sigma_b^2 + \sigma_t^2}$, which corresponds to $\frac{2,576}{T}\sqrt{N_b + N_t}$ for counts lasting for a time T. If the activity is low, $N_b \simeq N_t$ and $n_{sin} = \frac{3,6}{T}\sqrt{N_b}$. /59

The minimum rate detectable with a probability of 99%, with a noise rate of n_b and a measurement time of T, then becomes

$$\boxed{n_{sin} = 3.6\sqrt{\frac{n_b}{T}}} .$$

A family of curves $n_{sin} = f(T)$ can be drawn with n_b as parameter. These curves permit defining the time of measurement required to show the activity provided by the counting rate n_{sin} within the characteristic fluctuations n_b (Figure 50).

Since the detector yield is η, the minimum detectable activity is

$$A_{sin} = \frac{n_{sin}}{\eta} .$$

b. Comparison of the Two Photomultipliers 56 UVP and 56 AVP

This experiment was done with the tank painted white. The photomultipliers operated at 2300 volts under conditions close to the characteristic fluctuation. The measurement time was 10 minutes, and the activity $5\ 10^{-7}$ μc/cc of strontium-yttrium 90.

We obtained the following results for the counting rates in impacts per minute.

/58

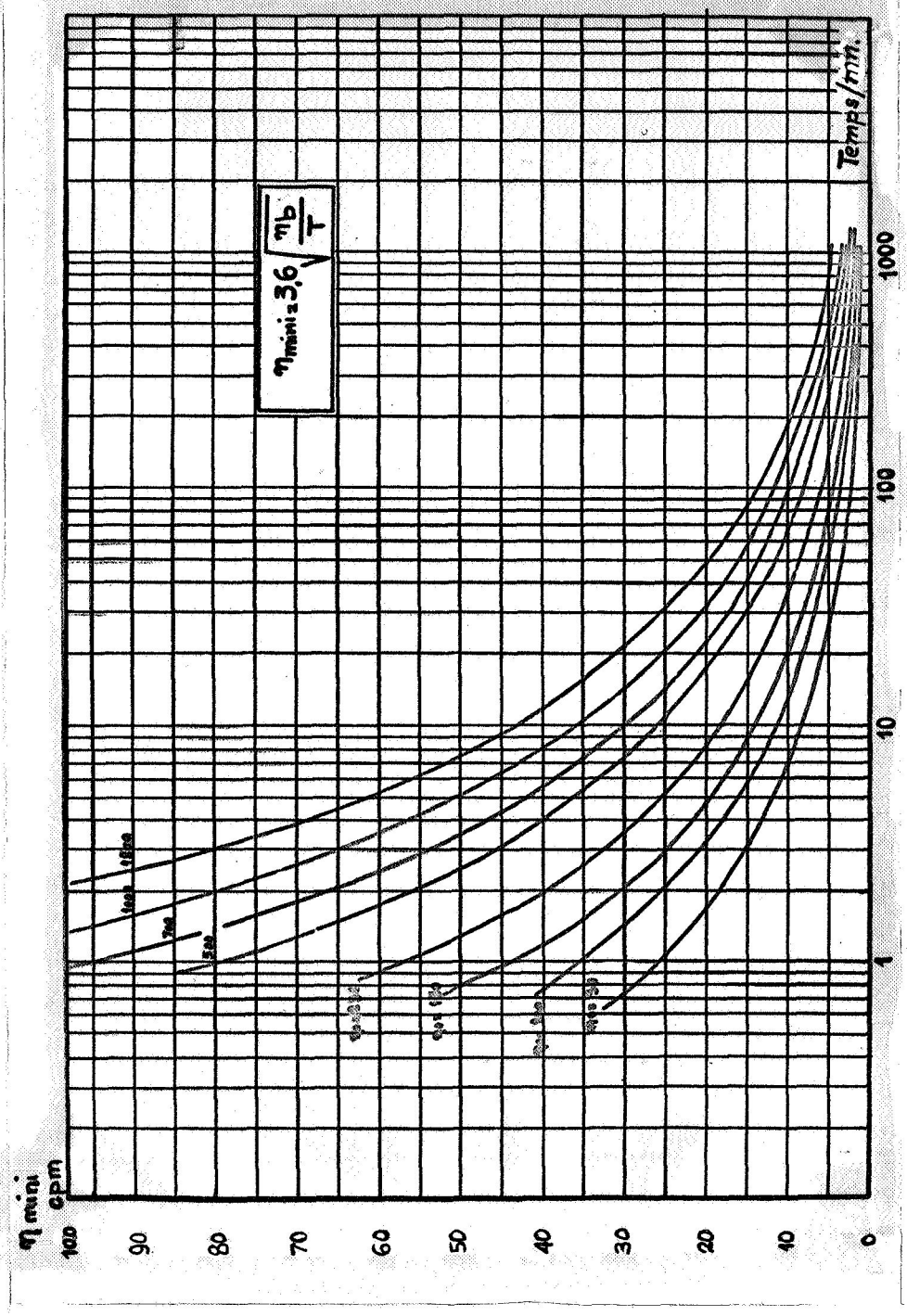

Figure 50. Least Number of Impacts Detectable.

P.M.	56 AVP	56 UVP
Chance coincidences	22	19
Characteristic fluctuations	255	210
Total rate	304	305
Signal	49	95
Yield, η, %	4.5	8.7

Under the conditions of the experiment, we found that the photomultiplier with a quartz window gives practically double the counting rate.

c. Comparison of Several Reflectors

We can compare three types of reflecting or diffusing materials: the white paint used for the various experiments, silvering, and aluminum foil which is not specially treated. All other factors – activity and the voltage applied to the 56 UVP's – are the same.

	Paint	Silver	Aluminum
Characteristic fluctuations	210	193	284
Signal	95	75	74
Yield, η, %	8.7	6.8	6.8

Unfortunately, the metals are attacked rapidly by the chemical action of the water. Moreover, the marked increase in the characteristic fluctuations for the aluminum foil seems to be due to the activity of the metal itself.

d. Detection of a Tenth of the Dose of Sr /60

The sensitivity may be improved by using anti-coincidence for the cosmic rays. The adjustable threshold permits eliminating pulses which overshoot a certain level. However, if this threshold is lowered too much, there is a possibility of suppressing signal pulse counts. A compromise is therefore required; we chose to keep 80% of the signal count.

For the detection of strontium, a given adjustment of the anti-coincidence circuit reduces the background noise to 75 cpm for the UVP in the lead housing. Under these conditions, the counting rate is 75 cpm for an activity of $5 \cdot 10^{-7}$ μ c/cc, which provides a yield of 6.8%. The tenth of the dose, corresponding to 180 dpm per liter, would be detected in seven minutes according to the family of curves (Figure 47). Without anti-coincidence and with a yield of 8.7 %, the time required for measurement would be 12 minutes.

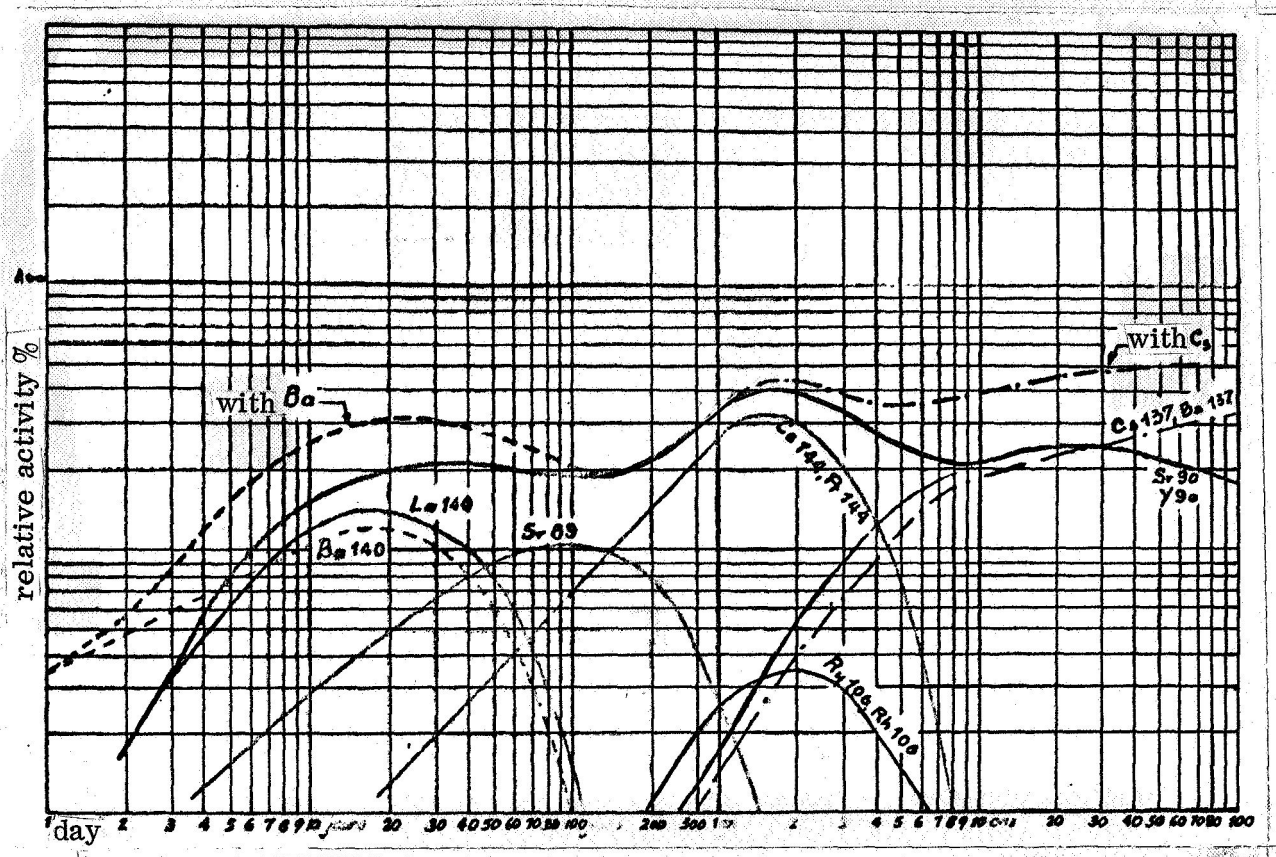

Figure 51. Percentage of Beta Activity Detectable by the Cerenkov Effect.

We can thus be sure of detecting the tenth of the Sr^{90} dose in drinking water with two tests of 10 minutes with equipment that requires no special treatment of the water such as dessication, vaporization, introduction of scintillating material, or converters. For turbid water, however, a preliminary filtration followed by a separate count for the filter is required.

5. Principle of Contamination Detection

/61

a. Fission Products Subject to Cerenkov Detection

Drinking water or rain water may be polluted by various radioactive materials emitting α, β, or γ radiation. Our equipment, however, permits only the detection of beta electrons with energies higher than 260 keV, the coincidence yield being no more than 20% except for energies higher than 600 keV. Rainwater contaminated by fallout of radioactive fission products has a composition that varies with time [26]. We are interested only in materials with beta disintegration energies higher than 500 keV. We present a relative activity curve for these fission products as a function of the measurement date with regard to beta emitters of sufficient energy such as:

La^{140}	2.2 MeV to 0.42 MeV
Sr^{89}	1.46 MeV

Ce^{144},	Pr^{144}	2.98 MeV
Ru^{106},	Rh^{106}	3.5 MeV
Sr^{90},	Y^{90}	2.2 MeV
Cs^{137},	Ba^{137}	0.51 MeV

(see Figure 51)

It has been established that the total beta activity varies at the most by a factor of two for periods between 20 days and 10 years. The maximum corresponds to one year and a half, where the activity is principally due to cerium-praseodymium 144, and is thus easily detectable. Beyond eight years, strontium and cesium are detectable with lower yield. In waste water that is relatively new (11 days), where the activity is due to strontium 89 and lanthanum 140, we can predict the final activity of strontium 90 with good approximation.

b. Calibrating the Detector

The detector yield for several beta emitters with very different maxima may be measured. For this purpose, cesium 137, strontium 90, potassium 40, and cerium 144 are used. The decay schemes of these elements are shown in Figure 52.

The activities used differ from the way in which the counting rates of the same order are obtained. For potassium, we use a potassium chloride solution containing 1.5 g of natural potassium. We thus obtain 45 betas per second. The anti-coincidence threshold is adjusted to a level corresponding to a background noise of about 70 cpm. In the table below, we have noted the percentage of the total count obtained with the use of anti-coincidence. Naturally, for substances of low energy, the anti-coincidence threshold as defined above has little effect.

The table shows the various counting rates in clicks per minute for the tank painted white. The detector is calibrated in the following way:

1) For a background noise reduced to 76 cpm by the anti-coincidence circuit, the ratio of the signal counting rate to the same counting rate without use of the anti-coincidence circuit is known. For each of the four substances, notable for the maximum energy of their beta spectrum, that rate is also known. We can thus draw the curve for the ratio $\frac{N_{s\ AC}}{N_{sT}}$ as a function of E_{max}. We obtain a curve for a given adjustment of the anti-coincidence which tends to 100% for energies of about 260 keV.

2) We know the total detection yield (without anti-coincidence) for each of the elements, and consequently the counting rate obtained for a given activity -- of $5 \cdot 10^{-6}$ μ c/cc or 11,000 dpm/liter, for example. We can thus draw a second curve for the yield as a function of the maximum energy of the beta spectrum.

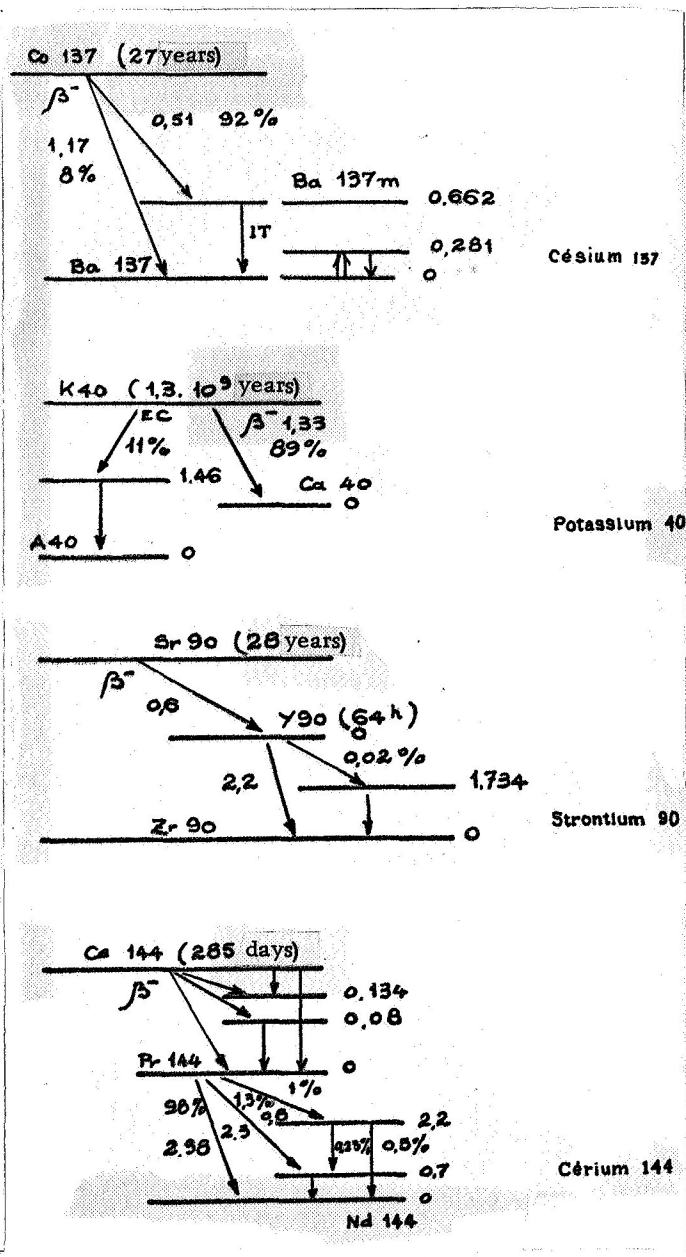

Figure 52. Decay Schemes.

c. Dosage in Water

/62

With the detector calibrated for energy using the two curves drawn, we can set the dosage in a particular water sample provided it has only a single beta-producing radioactive element. The procedure is then the following:

1) We determine the detector background noise for pure water (220 cpm).
2) We adjust the anti-coincidence threshold to reduce the noise to 75 cpm.
3) We then raise the counting rate $N_{s\ AC}$ with anti-coincidence. /63
4) We do the same for the total counting rate N_{sT}.

The ratio $\frac{N_{s\ AC}}{N_{s\ T}}$ in the curve of Figure 53 indicates the maximum energy of the beta rays emitted by the active element if we also know the detector yield for this energy.

The curve of Figure 54 gives us the counting rate obtained for 11,000 dpm/liter, equal to C. The activity of the water in dpm/liter is therefore

$$A\ \text{dpm/l} = 11,000 \times \frac{N_{ST}}{C}$$

or, in μc/cc,

$$A\ \mu\text{c/cc} = 5.10 \frac{N_{ST}}{C}.$$

The problem is obviously more complicated in the case of rainwater dosage, where the total activity is due to very different elements. As in every beta measurement, we cannot give absolute results because of the many varied yields, but we can indicate their energy and especially the variation of the total energy with time.

For more complete indications of the composition of beta emitters and their activities, one must have a family of $\frac{N_{s\ AC}}{N_{s\ T}}$ curves for various values of background noise or of threshold. For a higher threshold, $N_s Ac$ is higher since few pulses are /65

Substance and activity		Total count cpm	Count with anti-coincidence	Percentage $\frac{N_{s\,AC}}{N_{s\,T}}$
Cs^{137}	Noise	220	65	
$5.4 \cdot 10^{-6}$ μc/cc	Signal + noise	292	132	
equal to: 12000 dpm/l	Signal η p. 100	72 0.6	67 0,56	93 p. 100
K^{40}	Noise	220	75	
$1.2 \cdot 10^{-6}$ μc/cc	Signal + noise	333	165	
equal to: 2700 dpm/l	Signal η p. 100	113 4.1	90 3.3	82 p. 100
Sr^{90} - Y^{90}	Noise	210	75	
5.10^{-7} μc/cc	Signal + noise	305	150	
equal to: 1100 dpm/l	Signal η p. 100	95 8.7	75 6.8	79 p. 100
Cr^{144} - Pr^{144}	Noise	210	171	
$5 \cdot 10^{-7}$ μc/cc	Signal + noise	360	153	
equal to: 1100 dpm/l	Signal η p. 100	150 13.6	82 7.4	55 p. 100

Substance	Cs^{137}	K^{40}	Sr^{90}	Ce^{144}
Yield %	0.6	4.1	8.7	13.6
Counting rate for 5.10^{-6} μc/cc	66	500	960	1490
Maximumenerg MeV	0,55	1.3	2,2	2.98

reduced in anti-coincidence, and the ratio $\frac{N_{s\,AC}}{N_{s\,T}}$ tends rapidly to 100% at decreasing energies.

Suppose, for example, that we want to determine the dosage of water in which the activity is distributed equally between potassium 40 and praseodymium 144. Let us assume that each element gives 500 disintegrations per minute per liter. A family of curves for the threshold tells us, for example, that we should get a count of 50% of Pr^{144} and 70% of K^{40} for a particular threshold adjustment. With respective yields of 14% and 5%, we record 70 cpm from the Pr^{144} and 25 cpm from the K^{40}; i.e., a total of 95 cpm. In a count with anti-coincidence, we get 53 cpm, of which 35 come from the Pr^{144} and 18 from the K^{40}. This corresponds to 56% for the ratio $\frac{N_{s\,AC.}}{N_{sT}}$

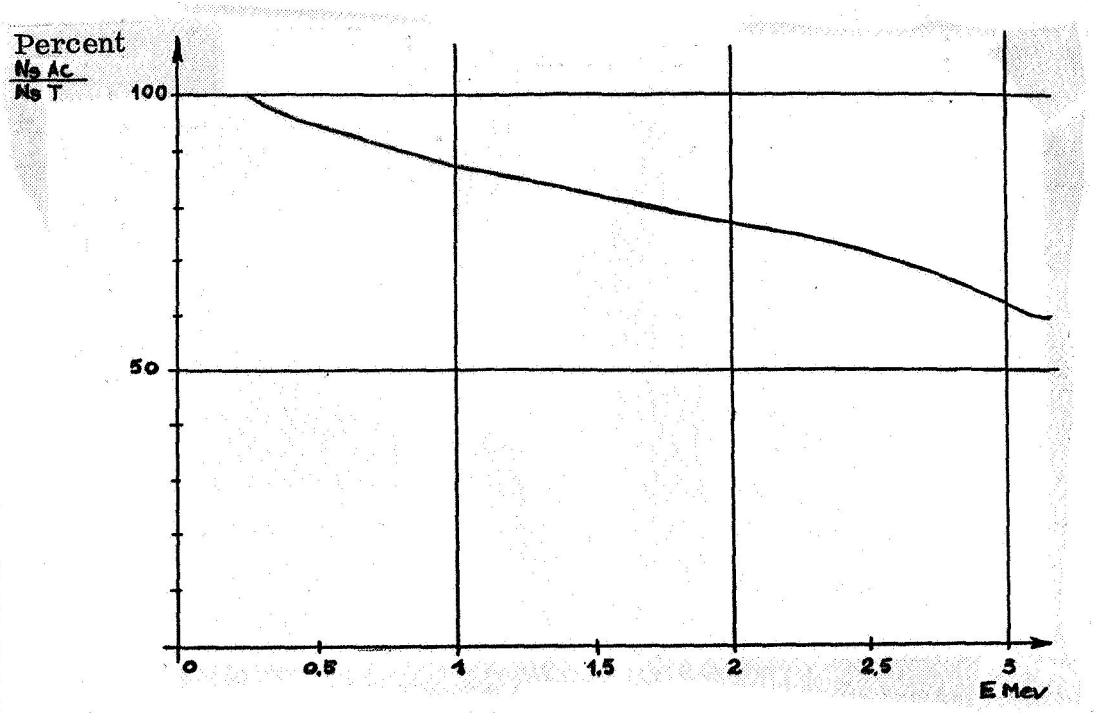

Figure 53. Example of the Efficiency of the Anti-coincidence Threshold.

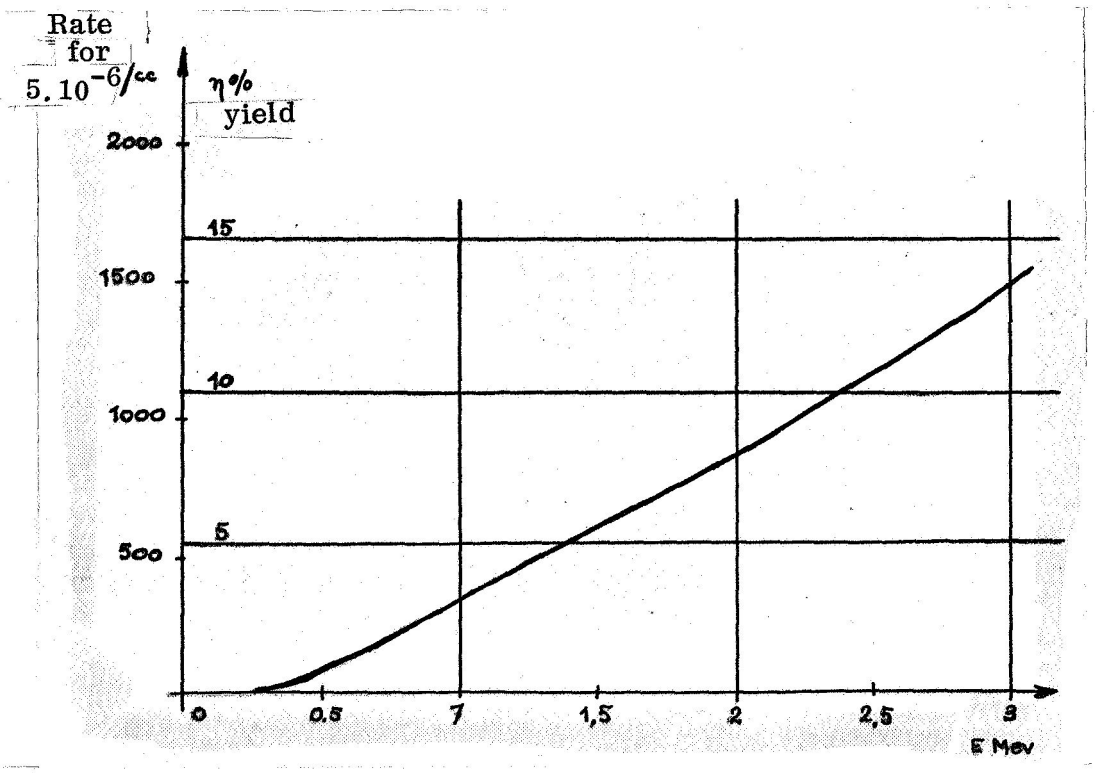

Figure 54. Curve of the Yield as a Function of the Energy.

This ratio indicates the existence of an element emitting beta rays of higher energy. But if we assume that the activity is the result of a single substance only, we will overestimate the detector yield and get a lower activity than is actually the case.

We have effectively verified this for a number of rainwater samples furnished to us and also tested by the CEN Grenoble Radiation Protection Service. Our equipment gave an underestimate. However, since the period of the rainwater was quite short (of the order of a month), we also managed to record a marked diminution in activity. The activities measured were of the order of one to $5 \cdot 10^{-7}$ μc/cc, and the five samples compared varied in the same direction, and did not differ by 10%.

Thus, a preliminary calibration of the detector permits determining, through rapid measurement, the amount of activity in rainwater. The variable threshold permits estimating the maximum energy of the emitted beta rays. We can then take this into account in evaluating the total activity, and especially of the activity of strontium 90, which may be underestimated if one attributes to the detector an excessively high yield for the total activity.

CONCLUSION

The contamination of running water from radioactive sources has several causes: atomic fallout brought to earth by rainwater; exhaust wastes from reactors or from factories working with radioactive materials. These products present some danger to life, and are particularly dangerous in the case of strontium 90, which settles in the bones. Standards for protection have been set: a tolerance of $8 \cdot 10^{-7}$ μc/cc for strontium 90 has thus been fixed for drinking water. /67

Various methods are used for the continuous control of water. These involve submerged Geiger counters or surface-proportional counters (of the MBLE or Maushart type) which permit detection at the CMA level. Other methods give better sensitivity by vaporization (ACRE 111, CEA type) or by dessication and scintillation counting.

Our equipment permits detecting $8 \cdot 10^{-8}$ μc/cc of strontium-yttrium 90 in water; i.e., a tenth of the maximum permissible concentration measured in a time of about ten minutes. It is especially useful for continuous water monitoring because of its simplicity of manufacture and operation. Moreover, the detector permits identification of the various elements in the water by the method of energy discrimination.

REFERENCES

1. Ducros, R. and G: Conference de Belgrade, Vol. I, p. 55, May 1961.
2. Takumi, K. and Yamada, S. Conference de Belgrade, Vol. III. p. 459, May 1961.
3. Pa. Cerenkov, Dokl. Akad Nauk SSSR, Vol. 2, p. 451, 1834.
4. Pa. Cerenkov, Dokl. Akad Nauk SSSR, Vol. 21, p. 319, 1938.
5. Frank and Tamm, Dokl. Akad Nauk SSSR, Vol. 14, p. 109, 1937.

6. Ginsburg V. L., Fiz. Zh. SSSR, Vol. 2, p. 441, 1940.
7. Properties of Ordinary Water, Remhod Publishing Corporation.
8. Taschenbuch fur, Chemiker and Physiker, Springer Verlag.
9. Les tubes photomultiplicateurs. (Photomultiplier tubes) S. A. La Radiotechnique.
10. Birks, J. B.: Scintillation Counters, Pergamon Press, 1953.
11. Segre, E.: Experimental Nuclear Physics, Vol. 1.
12. Breton, Denis: These Rapport, (Thesis), CEA No. 1198.
13. Katz and Penfold: Rev. Mod. Phys., Vol. 24, p. 28, 1952.
14. Breitenberger E.: Spectrometer fluctuation statistcs, Progress in Nuclear Physics, Vol. 4.
15. Hine and Brownell: Radiation Dosimetry, Academic Press.
16. Evans, R.D.: The Atomic Nucleus.
17. B. Jouve, Spectrographie gamma a grande sensibilite, (High-Sensitivity Gamma Spectrography), thesis, University of Paris, May 30, 1962.
18. Rossi, B: Rev. Mod Phys. Vol. 13 (4) 240.
19. B. Turck,: Rapport interieur non diffuse (Internal, undistributed report of the CEA).
20. J. Labeyrie,: Detection des rayonnements nucleaires, cours, (Course in Detection of Nuclear Radiation), Faculty of Sciences of Paris.
21. Goldanskii, VI. Counting Statistics of Nuclear Particles.
22. Kutzenko A. V: Pribory Tekh. Eksper. SSSR, Vol. 1, pp. 3-15, 1960.
23. Garwin: Rev. Sci. Inst., Vol. 24, p. 618, 1956.
24. Heiberg Marshall. Rev. Sci. Inst., 27, 618, 1956.
25. Porter, Nuovo Cimento: Vol. 5, p. 526, 1957.
26. Hunter, H. F. and Balloune: Nucleonics, Vol. 9, No. 5, C-2, Nov. 1951.
27. Brevet: (Patent) SAIP, No 1238828, July 7, 1959.
28. Brevet: (Patent) CEA PV 113044, October 22, 1962.

Translated for the National Aeronautics and Space Administration by Scripta Technica, Inc. NASw-1694.